TECHNICAL UNIVERSITY OF CRETE
SCHOOL OF ELECTRICAL AND CUMPUTER ENGINEERING

Transmit antenna selection among a linear array of plasma using MIMObit

by

Ioannis Giannakos

A thesis submitted in partial fulfillment of the requirements for the diploma degree of Electrical and Computer Engineering

THESIS COMITTEE
Professor George N. Karystinos , *Thesis Supervisor*
Professor Athanasios Liavas
Professor Nikolaos Kantartzis

July 2023

Acknowledgements

I would like to thank my supervisor, Professor George Karystinos, for his guidance and support throughout this work. Furthermore, i would to thank Ioannis Grypiotis for his support and constant help and Professors Athanasios Liavas and Nikolaos Kantartzis Special thanks to my family for their constant support throughout my studies. Finally, I would also like to thank my friends and Lambrina for the great time we spent together during this journey and the memorable moments we had through these 5 years in Crete.

Table of Contents

Table of Contents . . . 5

List of Abbreviations . . . 7

1 Introduction . . . 9

2 Monopoles, Radiation pattern, S-parameters . . . 11
2.1 Monopole Antennas . . . 11
2.2 Radiation pattern, S parameters . . . 14
2.2.1 Radiation pattern . . . 14
2.2.2 S-parameters . . . 16

3 Plasma antennas . . . 17
3.1 Antenna analysis and design . . . 20

4 Linear configuration and mutual coupling . . . 23
4.1 Linear Configuration . . . 23
4.2 Mutual Coupling . . . 25
4.2.1 Mutual Coupling, metallic antennas . . . 26
4.2.2 Mutual Coupling, plasma antennas . . . 28

5 Antenna selection and MISO . . . 29
5.1 Single Input Single Output antennas (SISO) . . . 29
5.2 Multiple Input Single Output antennas (MISO) . . . 32
5.3 Transmit Beamforming . . . 33
5.4 Antenna Selection . . . 35

6 MIMObit and CST . . . 37
6.1 Basics Overview . . . 38
6.2 Setup . . . 40

7 Experiments . . . 43
7.1 Experiment Description . . . 43
7.2 Channel Power . . . 45
7.3 Metallic/Plasma Antennas channel power over degrees for frequencies 500MHz, 550Hz, 600Hz . . . 76
7.4 Best performance based on channel power for 550MHz . . . 83

Bibliography 89

List of Abbreviations

AWGN	Additive White Gaussian Noise
MIMO	Multiple-Input Multiple-Output
SISO	Single-Input Single-Output
SNR	Signal to Noise-Ratio
LOS	Line-Of-Sight

Chapter 1

Introduction

In this study, we focus on investigating a linear array of metallic and plasma antennas in the context of multiple-input single-output (MISO) wireless systems. The data used for our analysis is generated using the specialized software MIMObit. Our objective of our research is to compare metallic and plasma antennas by implementing antenna selection in various scenarios.

We begin by providing an explanation of the functioning of monopoles and conduct a thorough analysis of their Radiation Pattern and S-parameter graphs. Subsequently, we explore the operation of plasma antennas, outlining their advantages and disadvantages.

The impact of the linear array configuration on antenna performance is thoroughly examined, as we analyze the phenomenon of mutual coupling for both metallic and plasma antennas. This phenomenon refers to the influence of one radiating monopole on the performance of others, and we study its effects on the overall antenna system.

Before entering the final chapter which contains the experiment setup, we explain the single-input single-output (SISO) and the multiple-input single-output (MISO) systems and how the antenna selection performs, and what we can achieve by this technique.

Using MIMObit, we utilize the channel coefficients to determine the channel power for each distinct case. Subsequently, we conduct a series of multiple experiments to observe and draw comparisons regarding the performance of both metallic and plasma antennas under various antenna selection scenarios. The outcomes of these experiments will enable us to draw valuable conclusions about the performance characteristics of the two antenna types.

Chapter 2

Monopoles, Radiation pattern, S-parameters

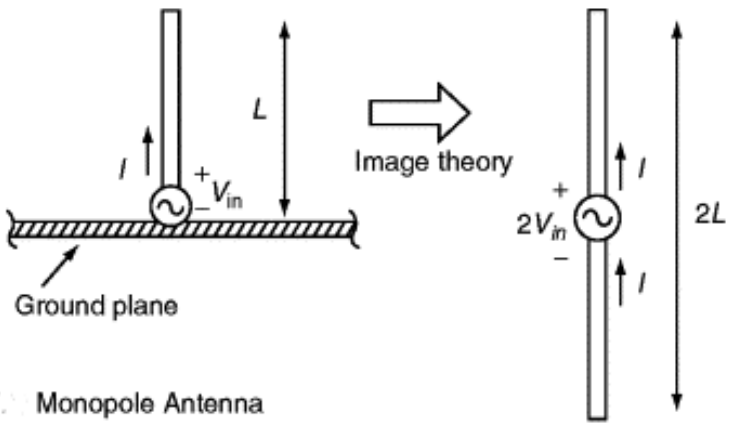

Figure 2.1: Monopole Antenna(The Electrical Engineering Handbook, "II - Antenna Elements and Arrays")

2.1 Monopole Antennas

Monopole antennas constitute a group of derivatives of dipole antennas. They were invented in 1895 by Guglielmo Marconi when he discovered that instead of using dipole antennas, the transmission signal could reach a further distance by connecting a wire to the transmitter and receiver on one side while mounting the other to the Earth.

More specifically, only half of the dipole antenna is needed for operation, and it is always mounted above some ground plane(ideally of infinite size), as depicted in Fig. 2.1. It consists of a conductor perpendicular to a ground plane and the presence of the ground plane allows the monopole antenna to operate as electrically equivalent to a dipole antenna. This contrasts with a dipole antenna which consists of two identical rod conductors, with the signal applied between the two halves of the antenna.

A similar half structure for a folded dipole antenna is called a folded monopole antenna, as depicted in Fig. 2.2. The ground plane equivalently replaces the lower half by an imaging principle, similar to creating an optical image through a mirror. It is essential to mention that the current between monopole and dipole structures is not the same, as the dipoles need twice the source voltage of the equivalent monopole ones. As a result, the input impedance of the monopole structure is half that of the corresponding dipole structure:

$$Z_{monopole} = \frac{1}{2} Z_{dipole}; Z_{monopole} = \frac{V_{in}}{I_{in}}, Z_{dipole} = 2\frac{V_{in}}{I_{in}}$$

In general, the length of the antenna is determined by the wavelength of the desired radio waves. The most common form is the quarter-wave which means that the antenna has a length equal to one-quarter of the radio waves wavelength. For a quarter-wave monopole with L=$\lambda_0/4$(the corresponding length of the equivalent dipole antenna is L=$\lambda_0/2$), the impedance is half of that of a half-wave dipole:

$$Z_{monopole} = \frac{1}{2} Z_{dipole} = 36.5\Omega$$

$$Z_{foldedmonopole} = \frac{1}{2} Z_{foldeddipole} = 146\Omega$$

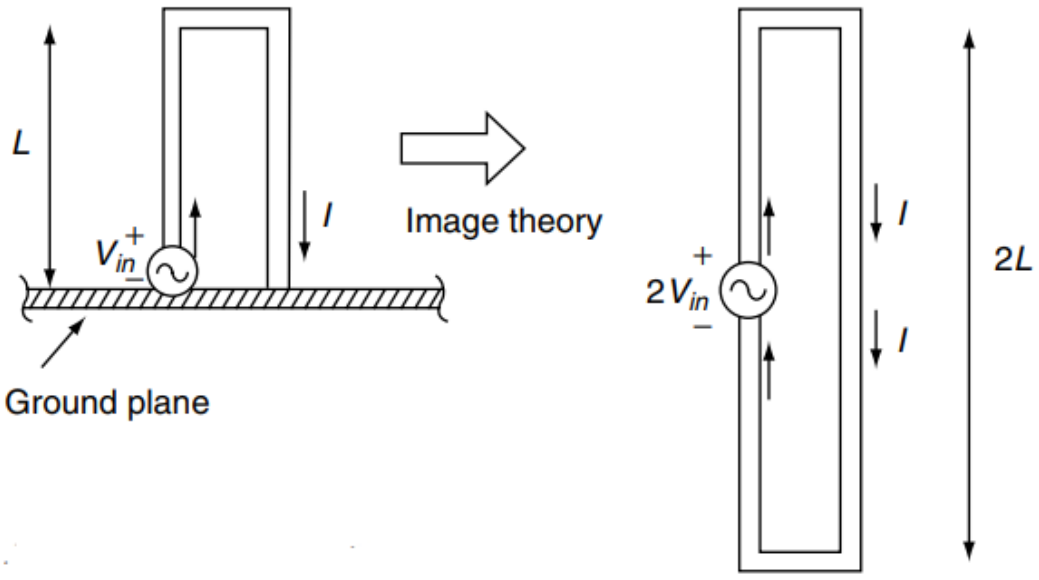

Figure 2.2: Folded Monopole Antenna(The Electrical Engineering Handbook, "II - Antenna Elements and Arrays")

It is reasonable because it requires only half the voltage to drive a monopole antenna with the same current as a dipole. Dipoles have +V/2 and -V/2 applied to their ends, while monopoles only need +V/2 and the ground plane to operate. Since Z_{in} = V/I, the impedance of the monopole antenna is halved.

Overall, monopole antennas have several advantages over other types of antennas. They are relatively easy to construct and can be mounted on various surfaces, including metal, wood, or plastic. They are also relatively inexpensive, small, and lightweight, which makes them ideal for portable applications. They can be used in various applications, such as mobile phones, GPS, WiFi, and Bluetooth applications. However, the monopoles have some disadvantages as well. They are less efficient than other antennas, such as dipole antennas, and they typically have limited bandwidth. They also tend to have a higher ground noise level, which can interfere with the signal.

2.2 Radiation pattern, S parameters

2.2.1 Radiation pattern

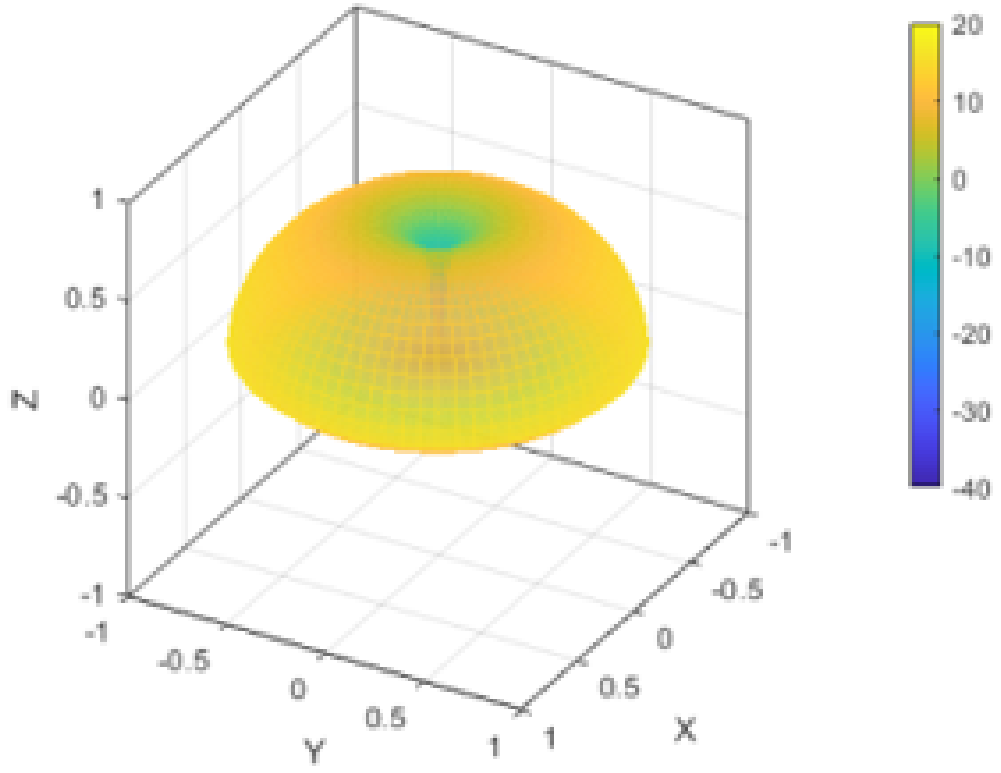

Figure 2.3: Monopole Radiation pattern

Radiation pattern in antennas refers to the directional distribution of energy emitted by an antenna. It describes how the energy radiated by an antenna is concentrated in different directions as a function of the position around the antenna. An antenna radiates energy from different parts in all directions around it. So, the radiation pattern is a three-dimensional figure and is represented as a function of spherical coordinates (r, ϑ, Φ), as depicted in Fig 2.3.
It is essential to mention that the radiation pattern of a monopole is highly affected by the size of the ground plane analyzed in the previous section.

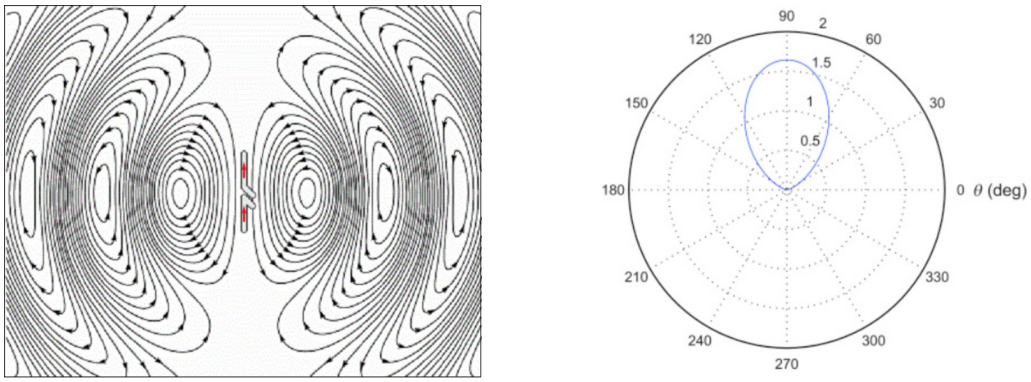

Figure 2.4: Monopole Radiation pattern(Antenna Theory - Radiation Pattern)

In Fig 2.4 and Fig 2.5, we can notice that it can also be represented as a two-dimensional system. The arrows point out the direction of the radiation.

Radiation from different parts of an antenna can lead to interference at some angles. These can result in zero radiation in several angles (where waves arrive out of phase) and local maxima (in parts where waves arrive in phase). The points where the maxima are observed are called "lobes" as depicted in Fig 2.5. It is ubiquitous for the radiation pattern to be described with lobe formation. The lobe that appears more extensive than others is called the "main lobe" and represents the direction in which the antenna is designed to radiate the most energy, while the lobe that is in the opposite direction (180°) is called the "back lobe".

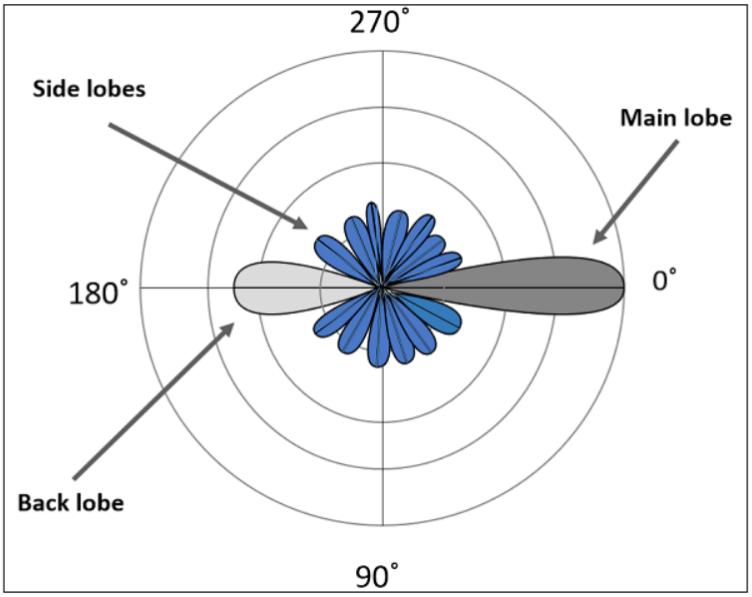

Figure 2.5: Lobe Formation(Antenna Theory - Radiation Pattern)

2.2.2 S-parameters

S-parameters describe an electrical system's input-output relationship between ports (or terminals). For example, in our study case, S-parameters represent the energy transferred between the four monopoles and how each one is affected. We use the notation:

$$S_{index\_of\_first\_monopole,index\_of\_second\_monopole}$$

For instance, S_{13} describes the energy transferred from monopole 1 to monopole 3. Fig. 2.6 shows how the S-parameters are plotted over **Frequency(MHz)** and **Magnitude(dB)** for monopole number 1. We can imply that the antenna will radiate best for plot S11 in 600MHz at approximately -25dB. In contrast, at 400MHz, the antenna will effectively emit negligible radiation.

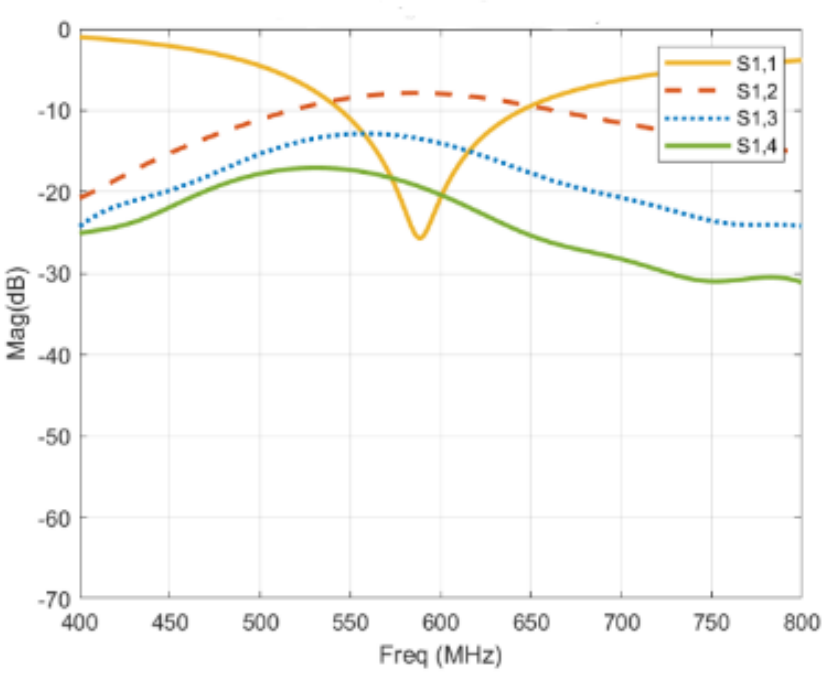

Figure 2.6: S-parameters

Chapter 3

Plasma antennas

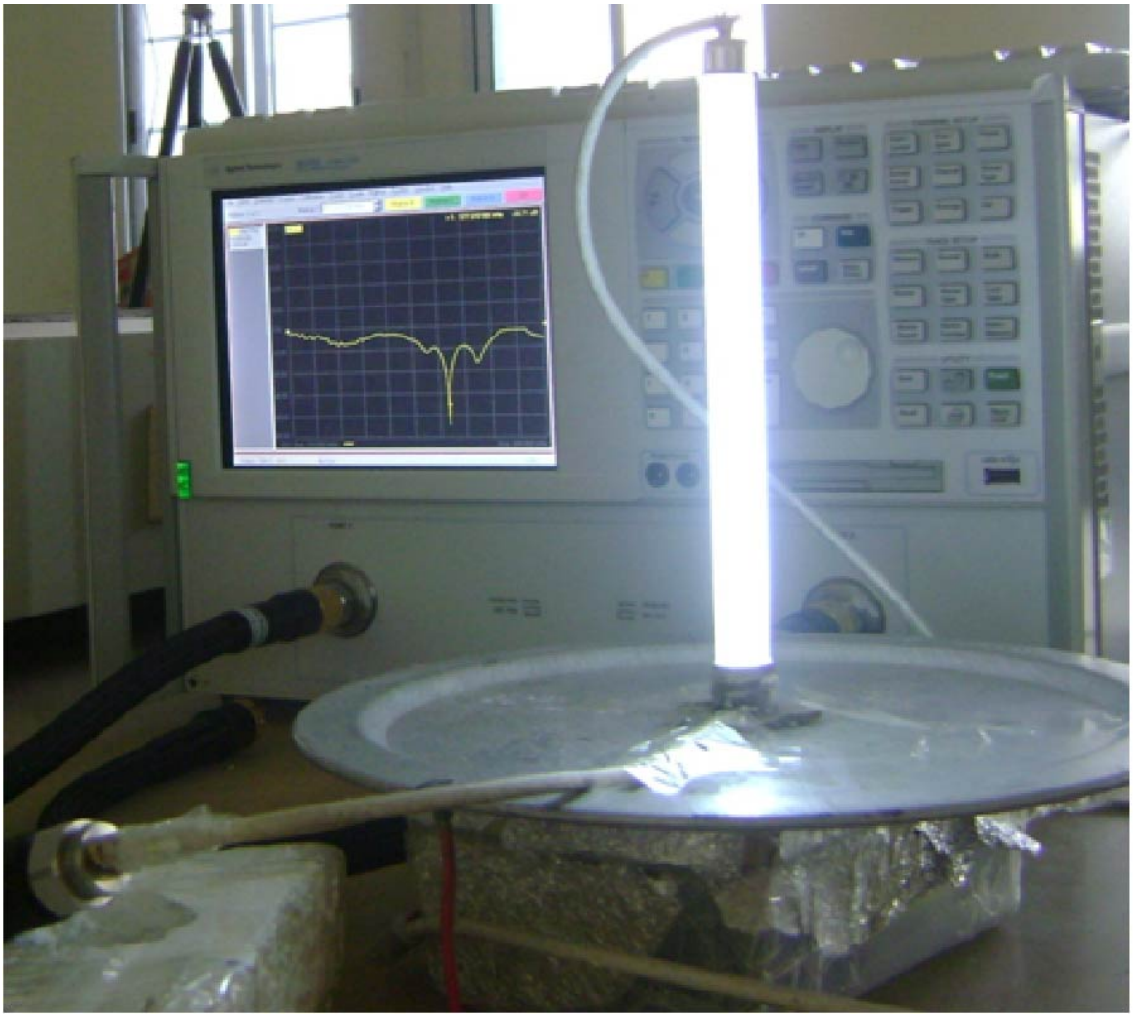

Figure 3.1: Plasma antenna(Study of a fluorescent tube as plasma antenna)

General

Plasma antennas are a relatively new type of antenna that uses ionized gas, or plasma, as the conducting element to generate electromagnetic radiation instead of metal. This allows for several unique properties and advantages over traditional metal antennas. Their potential is still being researched, and they can be utilized in various applications, including telecommunications, radar, and imaging.

Plasma antennas work by creating a plasma discharge within a small area, such as a tube or chamber. The plasma is formed by ionizing a gas, such as argon or helium, and then applying an electric field to the plasma, as seen in Fig. 3.3. The electromagnetic radiation produced by the plasma as a result of the electric field can be used for sensing or communication..

Advantages

One of the key advantages of plasma antennas is their ability to change shape and size in response to changes in the radio frequency (RF) signal being transmitted or received. This allows for a level of adaptability that is not possible with traditional metal antennas. Furthermore, they can be decreased in size and more compact than traditional antennas, making them useful for applications where space limitations are observed. They also have the potential to be more efficient and have a broader frequency range than traditional antennas. To be more specific, they have the ability to operate over a wide range of frequencies, from low-frequency radio waves to high-frequency millimeter waves. This makes them well-suited for various applications, including wireless communication, radar, and sensing. Additionally, they do not suffer from the same problems with corrosion and wear as traditional metal antennas, which can make them more durable over time. Last but not least, plasma antennas have a high resistance to interference from other electromagnetic sources, which makes them well-suited for use in environments where metal antennas may not perform as well. This makes plasma antennas a potential solution for applications in high-interference environments, such as in urban areas or with the presence of other electronic devices.

Disadvantages

However, there are some significant disadvantages as well. First of all, plasma antennas are generally more expensive due to their complex design, manufacturing process, and materials required for their operation. Furthermore, power consumption is a critical concern because of the fact that plasma antennas need a remarkable amount of energy in order to operate. To continue, there may be stability issues, especially in severe weather conditions such as high winds or extreme temperatures. One last drawback could be that the plasma inside the antenna tube needs to be carefully and constantly controlled to ensure that it remains in the correct state for the antenna to function effectively.

Conclusion

Plasma antennas are still a relatively new technology and are not yet widely used in commercial applications. Further research is needed to improve their performance and reliability before they can be adopted for widespread use. Some challenges researchers face with plasma antennas include developing methods to maintain a stable plasma discharge, controlling the frequency of the emitted radiation, and improving the antenna's efficiency. Overall, plasma antennas are a captivating area of research that holds the potential to revolutionize the field of antennas and wireless communications. In conclusion, plasma antennas are a promising new technology that offers several advantages over traditional metal antennas. Although there are still challenges to overcome, plasma antennas have the potential to provide better performance in various applications, including in high-interference environments, compact electronic devices, and wireless communication.

3.1 Antenna analysis and design

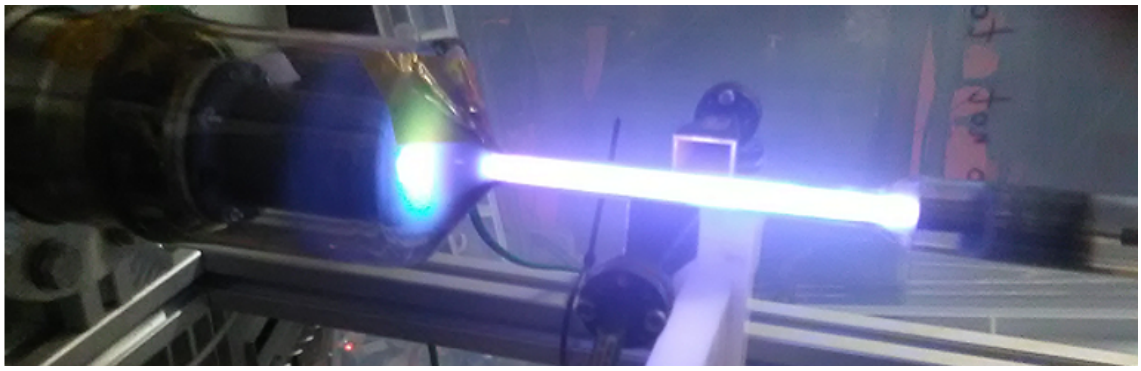

Figure 3.2: Hollow-Cathode plasma discharger

During Padovas 2018 workshop, it was extensively discussed and determined that the below two antenna setups are more convenient:

- Ground plane, quarter-wave monopole antenna
- Half-wave dipole antenna.

Because of their simple construction, they are considered more suitable and more proper for transmitting and receiving. Further, they are easily tested, and the results tend to be more precise (e.g., radiation pattern).
Moreover, we will examine the **Hollow Cathode (HC)** plasma source and its utilization as an antenna (Fig 3.2, 3.3).

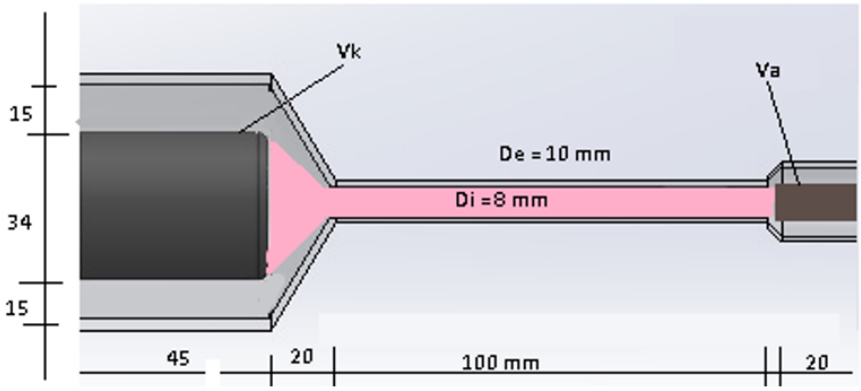

Figure 3.3: Layout of the Hollow-Cathode plasma discharger

In order to compute the electromagnetic parameters (ε,σ) we will use the Drude model as shown below:

$$\bar{\bar{\varepsilon}}(\omega) = \varepsilon_0 \begin{pmatrix} \varepsilon_1(\omega) & \varepsilon_2(\omega) & 0 \\ -\varepsilon_2(\omega) & \varepsilon_1(\omega) & 0 \\ 0 & 0 & \varepsilon_3(\omega) \end{pmatrix}$$

$$\varepsilon_1(\omega) = \varepsilon_\infty - \frac{\omega_p^2(\omega - i\upsilon_c)}{\omega(\omega - i\upsilon_c)^2 - \omega\omega_b^2} \quad \text{and} \quad \varepsilon_2(\omega) = \frac{-i\omega_p^2\omega_b}{\omega(\omega - i\upsilon_c)^2 - \omega\omega_b^2}$$

$$\varepsilon_3(\omega) = \varepsilon_\infty - \frac{\omega_p^2}{\omega(\omega - i\upsilon_c)} \quad \text{where} \quad \omega_b = \frac{eB_0}{m_e}$$

Figure 3.4: Drude model for the computation of complex electrical permittivity

By using (4.1), we can calculate the plasma's relative complex permittivity, whose real and imaginary parts correspond to its electric permittivity ε and conductivity σ, respectively

$$\bar{\varepsilon} = 1 - \frac{\omega_p^2}{\omega(\omega - jv_c)} \tag{3.1}$$

where ω is the angular frequency, v_c is the collision frequency and the plasma frequency ω_p can be calculated using the:

$$\omega_p = \sqrt{\frac{n_e q_e^2}{e_0 m_e}} \tag{3.2}$$

where n_e is the designating plasma frequency, e_0 is the electric permittivity of vacuum and m_e is the electron mass while q_e is the electron charge.
By using the Krook lumped model as a sum, we can calculate the collision frequency:

$$v_c = v_{en} + v_{ei} + v_{ie} \tag{3.3}$$

where ν_{en} symbolizes the electron-neutral collisions, and e and i are the indices of electrons(e) and ions(i).
The expressions for these collisions are

$$\begin{aligned} v_{en} &= 2.336 \cdot 10^{-14} T_e^{1.609} e^{0.0618(\ln T_e)^2 - 0.1171(\ln T_e)^3} \\ v_{ei} &= 2.91 \frac{n_e}{T_e^{3/2}} \left[23 + \ln\left(\frac{T_e^{3/2}}{\sqrt{n_e}} \right) \right] \\ v_{ie} &= 4.8 \cdot 10^{-2} \frac{1}{\sqrt{m_i}} \frac{n_e}{T_e^{3/2}} \left[23 + ln(\frac{T_e^{3/2}}{\sqrt{n_e}}) \right] \end{aligned} \tag{3.4}$$

where the plasma density n_e is expressed in m-3 and electron temperature Te in V.

Taking into consideration the above mathematical relationships and conclusions, it

was decided that the hollow cathode plasma source can be modeled as a ground plane, quarter-wave monopole antenna (Fig. 3.5).

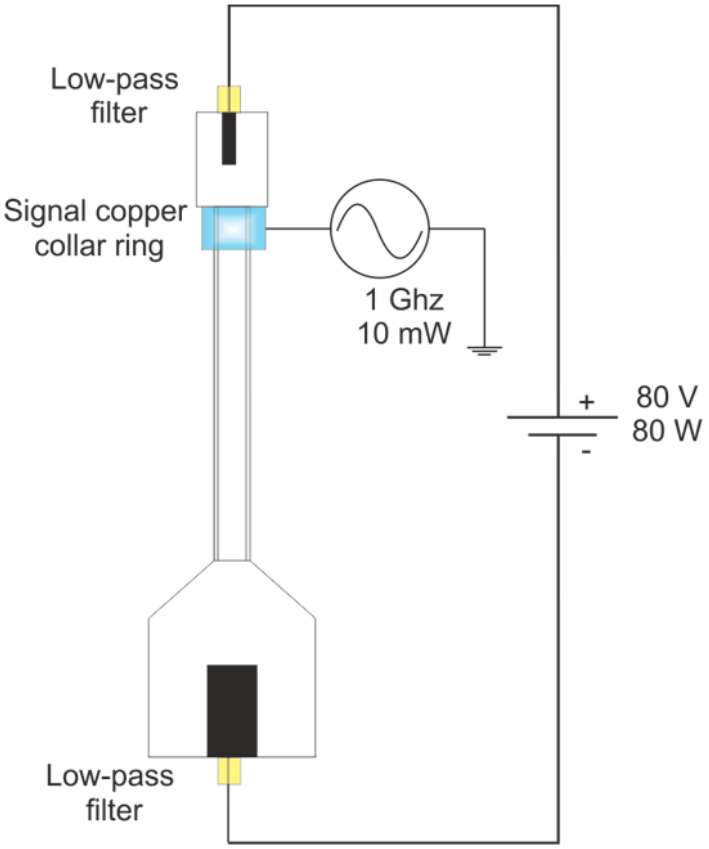

Figure 3.5: Hollow-cathode ground plane, quarter-wave monopole antenna.

Chapter 4

Linear configuration and mutual coupling

4.1 Linear Configuration

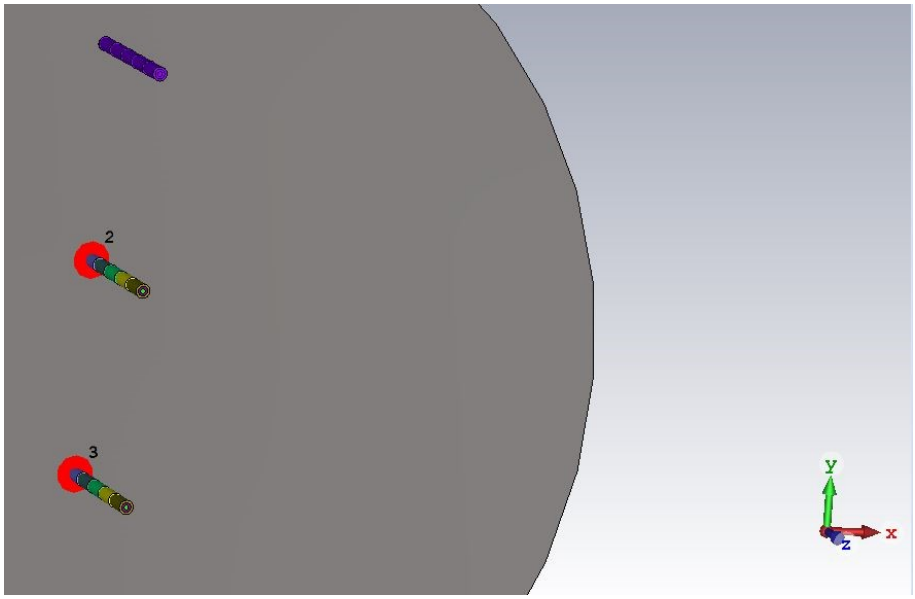

Figure 4.1: Linear configuration

In the previous Chapter, we delved into monopole antennas, then analyzed how they work and compared them to dipole antennas. In this section, we will examine the linear configuration, which involves the introduction of a set or array of monopoles in an antenna.

A linear antenna configuration arranges antenna elements along a straight line. This type of configuration is commonly used in various applications such as broadcasting, wireless communication, radar, and satellite communication. There are others, such as rectangular configuration, which defer from the linear in s-parameters, radiation patterns, etc.

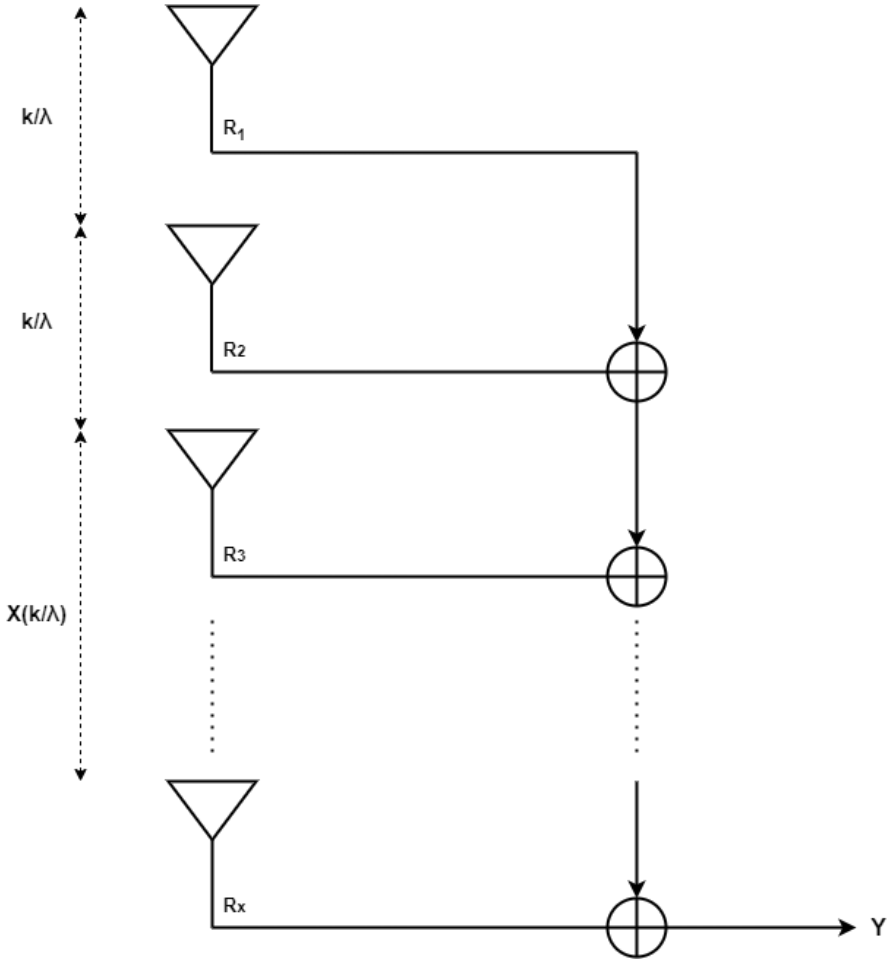

Figure 4.2: Antenna array system

An antenna array, alternatively referred to as a "phased array," encompasses a range of transmit antennas, starting from $N_t = 2$ and extending to an infinite number. The signals from the antennas are combined or processed to achieve improved performance over that of a single antenna.
Hence, combining N antennas provides the system with a higher antenna gain, increases signal strength, and obtains high directivity. Furthermore, it is essential to mention that minor lobes (discussed in the previous Chapter) are reduced while high SNR is achieved.

In Fig. 4.2, an antenna array system is presented where the output **Y** is a sum of all the receiver antennas. It is important to notice that the space between the monopoles is a multiple of the wavelength λ. For instance, in our experiments (Chapter 7), we drive results for an antenna array consisting of four monopoles using four different distances:

- $d = 0.24\lambda(12\text{cm})$
- $d = 0.32\lambda(16\text{cm})$
- $d = 0.40\lambda(20\text{cm})$
- $d = 0.48\lambda(24\text{cm})$

4.2 Mutual Coupling

Mutual coupling is a phenomenon that occurs when two or more antennas are placed next to each other, and their electromagnetic fields interact with one another. The effect of mutual coupling can be both constructive and destructive, and it can significantly impact the performance of the antennas. When two antennas are close, their electromagnetic fields interact, which can lead to energy transfer between the antennas. This energy transfer can increase or decrease the gain and directivity of the antennas, and it can also affect the impedance and radiation pattern of the antennas.

To ensure efficient radiation of an antenna, all the resistance around it (resistors, lossy dielectrics) must be removed. Nevertheless, when an antenna is placed close to the radiating one, it can cause a loss of power, known as **antenna coupling** or **mutual coupling**. Furthermore, the desired bandwidth is decreasing, and antennas have been observed to shift, which causes losses in direction.

Moreover, as we will notice in the following pages, significant changes regarding radiation patterns and S-parameters are being detected.

4.2.1 Mutual Coupling, metallic antennas

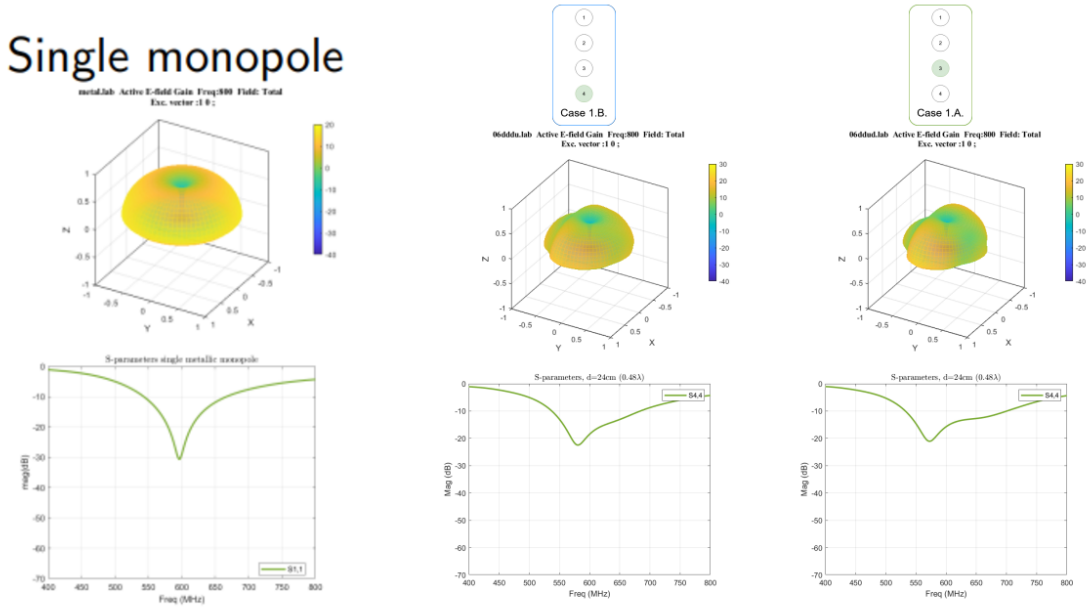

Figure 4.3: Radiation pattern, S-parameters for metallic case

In order to clarify our statement, we will use some graphic designs from our experiments. Using an antenna array of four monopoles, only one of them is radiating. In Fig. 4.3, we use three cases: single monopole case, case 1.B, and case 1.A where only the fourth and the third monopole are radiating, respectively.

In the first row, the radiation pattern of each case is presented. As discussed in the previous chapters, radiation pattern refers to the directional distribution of energy emitted by an antenna. In the first case, where only a monopole is radiating, the radiation pattern is even on all sides. When an antenna array is introduced, the formation mentioned above changes exceptionally. For instance, in both Case 1.A and Case 1.B, the radiation pattern schema presents anomalies, although only one of the four monopoles radiates. Therefore, even if the other monopoles are not radiating, they still affect the radiating one.

Next, it is crucial to comment on the S-parameters graphical that can be seen below of the radiation pattern ones. In Chapter 2, S-parameters were referred to as the description of the input-output relationship between ports of an antenna. Similar to the radiation pattern case, it is evident that S-parameters' graphical representation changes over the cases.

When the metallic monopoles are switched off, they still affect the radiating one. We can notice throughout the radiation pattern and S-parameters graphs that they affect the

radiation to a large extent. This can impact antenna gain and shift the antennas as well.

4.2.2 Mutual Coupling, plasma antennas

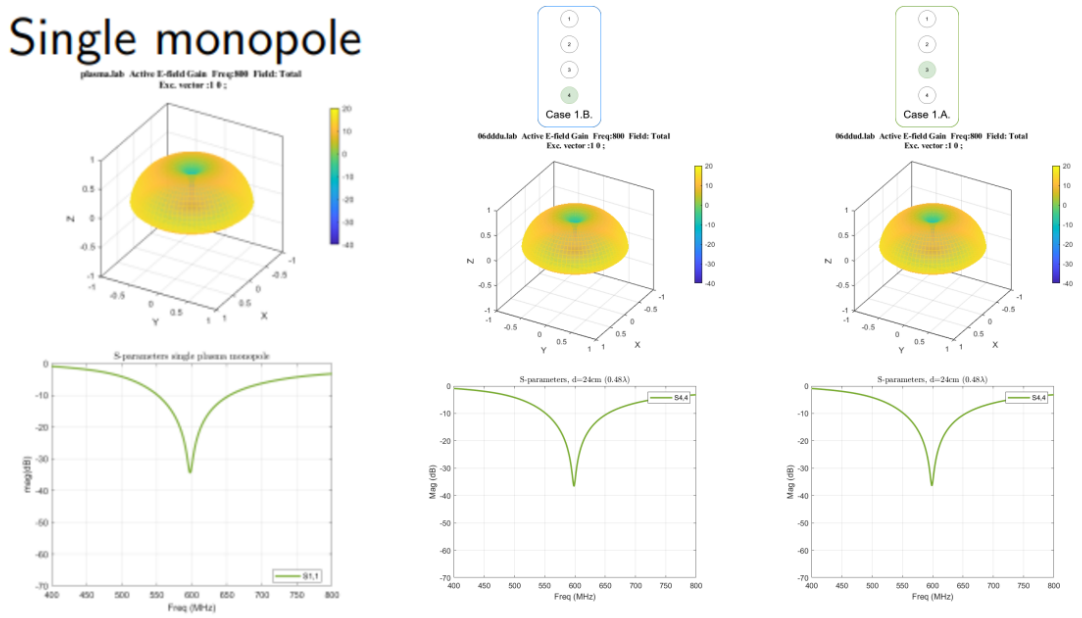

Figure 4.4: Radiation pattern, S-parameters for plasma case

On the other hand, in Fig. 4.4, we examine three cases: single monopole case, case 1.B, and case 1.A where only the fourth and the third monopole radiate, respectively, but this time we utilize plasma antennas compared to the metallic ones from the previous section. As we can seamlessly observe, neither the radiation pattern nor S-parameters change. Remarkably, the graphs remain the same as the single monopole case, even when more monopoles are used.

Therefore, even when utilizing extensive antenna arrays surpassing the magnitude of the four monopoles depicted in the figure., the other monopoles do not affect the operation of the radiating one.

General Conclusion

Metallic antennas are typically made of conductive metal. Their metallic properties and electromagnetic field affect the antenna's operation in total, even when not radiating. This is the reason we can see changes in the graphs. In contrast, plasma antennas are made of a gas-filled chamber, which is ionized by applying a high voltage to the gas. If we terminate the voltage, the antenna will stop "acting as an antenna" because it becomes neutral when the gas is not ionized. Thus, no changes are detected in the radiation pattern and S-parameters.

Chapter 5

Antenna selection and MISO

5.1 Single Input Single Output antennas (SISO)

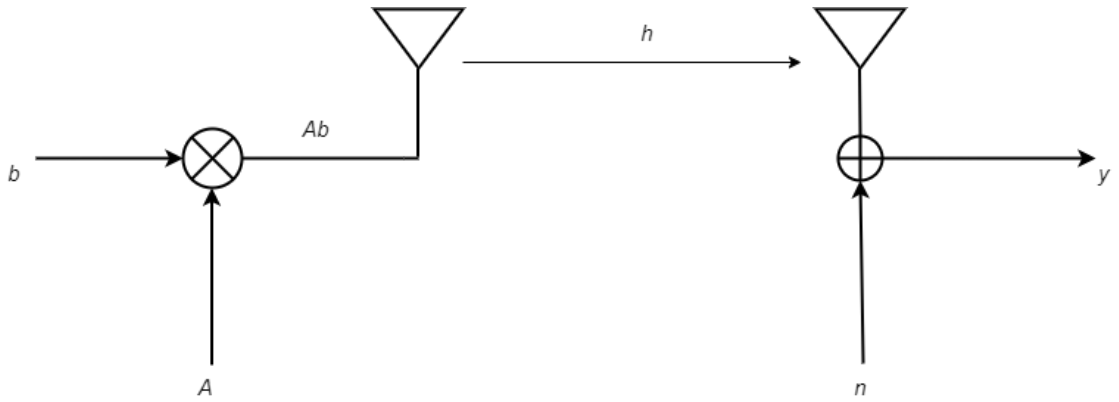

Figure 5.1: SISO system

A SISO system for single-input-single-output describes a system consisting of 1 transmit antenna and 1 receive antenna, as depicted in Fig 5.1. It is more than clear that the above figure illustrates a system that can be described with the below mathematical relationship:

$$y = Ahb + n \tag{5.1}$$

- b is the uniformly distributed bit $b = \pm 1$
- A is the amplitude, $A > 0$
- $h \in \mathbb{C}$ is the channel coefficient
- flat fading propagation
- n is the additive white Gaussian noise (AWGN), $n \sim \mathbb{CN}(0, \sigma^2)$

The optimal detector for a SISO system is given below:

$$Re(h^* y) \underset{\text{b=-1}}{\overset{\text{b=1}}{\lessgtr}} 0 \tag{5.2}$$

Finally, the probability of error is:

$$P_e = Q\left(\sqrt{2|h|^2 \frac{A^2}{\sigma^2}}\right) \tag{5.3}$$

Propagation Model

The above simple SISO system can be described as a simple **Line of Sight(LOS)** propagation model. The Line of Sight (LOS) propagation model is a simplified model for predicting the propagation of electromagnetic waves between antennas when they are in direct view of each other with no obstacles in between (they are in "direct line-of-sight" with each other). In this model, it is assumed that the transmitting and receiving antennas are located on flat ground, with no obstacles between them. In Fig 5.2, a simple LOS SISO system is presented:

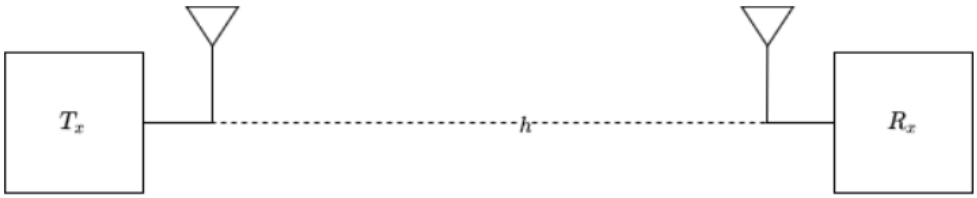

Figure 5.2: LOS SISO system

The output can be expressed as $y = hx$, with x being the input, h being the channel coefficient, and the channel power being defined as $|h|^2$.

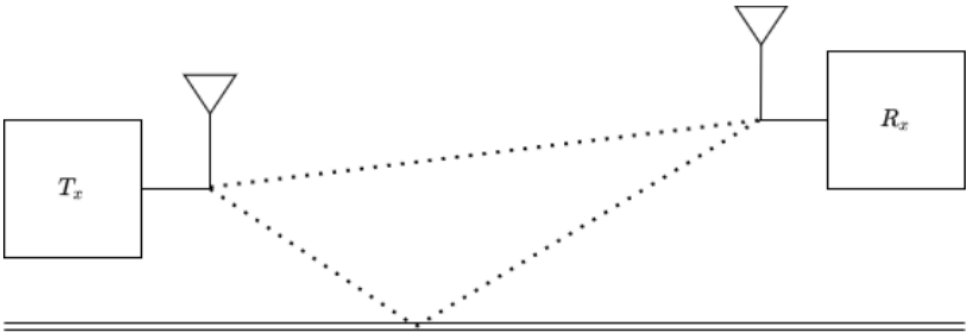

Figure 5.3: 2-Ray LOS SISO system

In Fig. 5.3, the 2-Ray propagation model is presented. As it is easy to comprehend, the 1-Ray model is being used to understand the theory more deeply to figure out what is happening in an ideal world. The 2-Ray model manifests that multiple rays can be transmitted. Some of them will not reach the receiver antenna R_x; some will reach the destination through a straight line, while others will reflect in some objects (e.g., walls) to access the receiver.
Output ($y = hx$), input (x), channel coefficient (h), and channel power ($|h|^2$) remains the same as explained in the above example (LOS).

5.2 Multiple Input Single Output antennas (MISO)

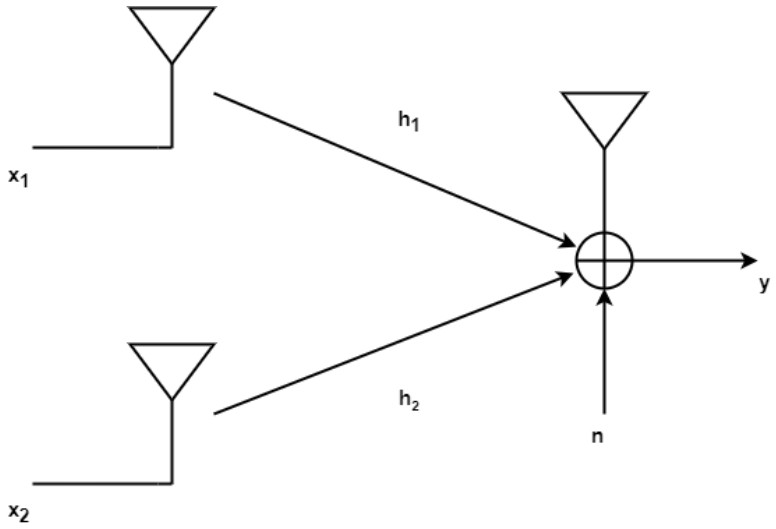

Figure 5.4: MISO 2×1 system

A MISO system which stands for multiple-input-single-output describes a system of antennas that consists of **n** transmit antennas, and 1 receive antenna. In Fig 5.4, a MISO 2×1 system is introduced. The above schema can be translated as:

$$y = \begin{bmatrix} h_1 & h_2 \end{bmatrix} \times \begin{bmatrix} x_1 \\ x_2 \end{bmatrix} + n = \mathbf{hx} + n \tag{5.4}$$

- $\mathbf{h} \in \mathbb{C}^{N_t}$ is a complex 1 x N_t vector that contains the channel coefficients, where N_t is the number of the transmitted antennas,
- $\mathbf{x}$ is a N_t x 1 vector that contains the transmitted symbols x_1, x_2,...,x_{N_t} ,
- n is the additive white Gaussian noise (AWGN) with $n \sim \mathcal{CN}(0, \sigma^2)$.

5.3 Transmit Beamforming

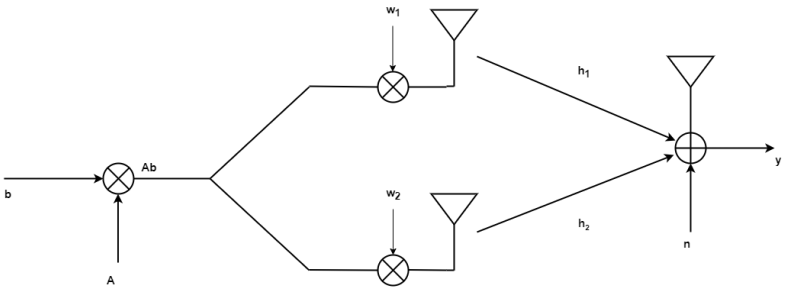

Figure 5.5: Transmit Beamformer 2×1 system

A Transmit Beamforming system is described in Fig. 5.5. The bit $\mathbf{b}=\mathbf{1}$ is multiplied by the amplitude $\mathbf{A}$. Then, a complex vector $\mathbf{w}$ is placed in the transmitting antenna in order to send the symbol. The above schema can be translated as:

$$y = \begin{bmatrix} h_1 \, h_2 \end{bmatrix} \begin{bmatrix} Abw_1 \\ Abw_2 \end{bmatrix} + n = A\mathbf{h}\mathbf{w}b + n$$

where:

$$\mathbf{x} = Ab\mathbf{w}$$

- b is the uniformly distributed bit with $b = \pm 1$,
- A is the amplitude with $A > 0$,
- $\mathbf{w}$ is a weight vector with $\mathbf{w} \in \mathbb{C}^{N_t}$, where N_t is the number of the transmit antennas and $\mathbb{C}$ N_t x 1 complex vector
- $\mathbf{h} \in \mathbb{C}^{N_t}$ is a complex 1 x N_t vector that contains the channel coefficients, where N_t is the number of the transmitted antennas,
- n is the additive white Gaussian noise (AWGN) with $n \sim \mathcal{CN}(0, \sigma^2)$.

For a fixed vector $\mathbf{w}$ in the optimal detector equation the $\mathbf{hw} \in \mathbb{C}$ is equivalent to $\mathbf{h} \in \mathbb{C}$ from (5.1). So, the (5.2) is described as:

$$Re((hw)^* y) \underset{\text{b=-1}}{\overset{\text{b=1}}{\lessgtr}} 0 \tag{5.5}$$

and the probability of error P_e is:

$$P_e = Q\left(\sqrt{2|\mathbf{hw}|^2 \frac{A^2}{\sigma^2}}\right) \tag{5.6}$$

Since w is a design parameter, we can optimize it to minimize the probability of error of the optimal detector. Since we have set the constraint $\|w\| = 1$, the optimal weight vector is:

$$\mathbf{w}_{opt} = \underset{\|w\|=1}{\operatorname{argmin}} P_e = \underset{\|w\|=1}{\operatorname{argmin}} |\mathbf{hw}| = \underset{\|w\|=1}{\operatorname{argmax}} \frac{|\mathbf{hw}|}{\|\mathbf{w}\|} \tag{5.7}$$

Using Cauchy-Scwartz Inequality,

$$\frac{|\mathbf{hw}|}{\|\mathbf{w}\|} \leq \frac{\|\mathbf{h}\|\|\mathbf{w}\|}{\|\mathbf{w}\|} = \|h\| \tag{5.8}$$

where equality exists if and only if $\mathbf{w} = \lambda \mathbf{h}^H$, $\lambda \in \mathbb{C} - \{0\}$. That is, equality holds if $\mathbf{w} = \frac{\mathbf{h}^H}{\|\mathbf{h}\|}$. Hence,

$$\mathbf{w}_{opt} = \frac{\mathbf{h}^H}{\|\mathbf{h}\|} \tag{5.9}$$

For the optimal vector $\mathbf{w}_{opt}$ the optimal detector is given by:

$$Re(y) \underset{\text{b=-1}}{\overset{\text{b=1}}{\lessgtr}} 0 \tag{5.10}$$

and its probability of error becomes:

$$P_e = Q\left(\sqrt{2\|\mathbf{h}\|^2 \frac{A^2}{\sigma^2}}\right) \tag{5.11}$$

5.4 Antenna Selection

Multiple-input multiple-output (MIMO) systems previously discussed in this chapter, can involve many monopoles or dipoles integrated into a single antenna structure. While the production of monopoles and dipoles is generally considered cost-effective, it is important to acknowledge that their implementation also entails a level of hardware complexity(RF circuits for every single port) that is not inexpensive. The radio front end's complexity, size, and cost are directly proportional to the number of antennas employed. However, mitigating these factors and simultaneously achieving many of the advantages associated with MISO systems is feasible by implementing **antenna selection** techniques.

Generally, the antenna will select the antenna port or a combination of ports that causes the **Signal to Noise Ratio (SNR)** or the **capacity** to be maximum. In **Chapter 7-Experiments**, we will perform antenna selection in a high extension. Utilizing a set of $N_t = 4$ antenna ports, we will perform antenna selection and examine every possible combination. Afterward, we will decide which antenna selection performs better for each case and draw the necessary results.

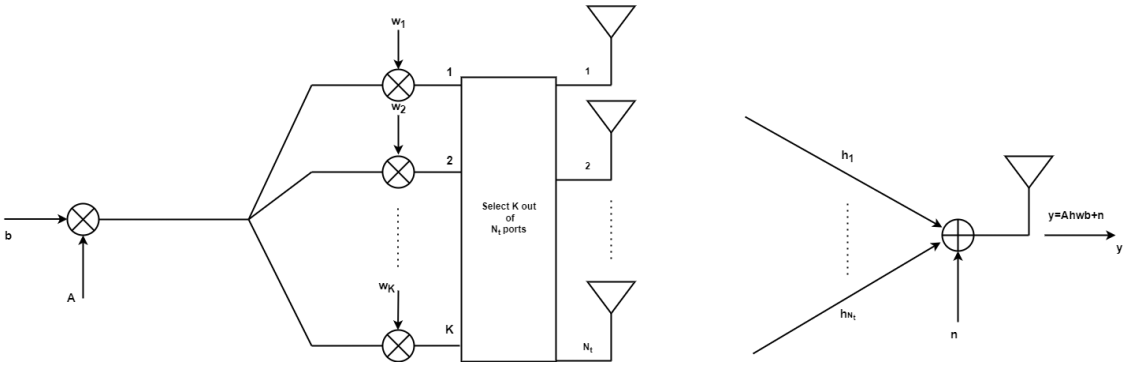

Figure 5.6: Antenna selection schema for a MISO system

In the given illustration (Figure 5.6), we examine a simple scenario of a MISO (Multiple-Input Single-Output) system with $N_r = 1$ receiving antenna and N_t transmit antennas. Our objective is to choose K transmit antennas from the total N_t antennas. When all N_t transmit antennas are employed, the received signal is as follows:

$$y = A\mathbf{h}\mathbf{w}b + n \tag{5.12}$$

Upon selecting K out of the available N_t transmit antennas, we identify the K indices corresponding to the chosen antennas. Subsequently, the received signal can be expressed as follows:

$$\tilde{y} = \tilde{\mathbf{h}}\tilde{\mathbf{w}}b + n \tag{5.13}$$

where $\tilde{\mathbf{h}}$ is 1 x K and $\tilde{\mathbf{w}}$ is K x 1

Before the antenna selection, the optimal detector is

$$Re((hw)^{*}y) \underset{\text{b=-1}}{\overset{\text{b=1}}{\lessgtr}} 0 \tag{5.14}$$

and its probability of error is

$$P_e = Q\left(\sqrt{2|\mathbf{hw}|^2 \frac{A^2}{\sigma^2}}\right) \tag{5.15}$$

After K antenna elements are selected, the optimal detector is

$$\mathrm{Re}((\tilde{\mathbf{h}}\tilde{\mathbf{w}})^{*}\tilde{y}) \begin{cases} \geq 0, & \text{if } b = 1, \\ < 0, & \text{if } b = -1. \end{cases} \tag{5.16}$$

and its probability of error is

$$P_e = Q\left(\sqrt{2|\tilde{\mathbf{h}}\tilde{\mathbf{w}}|^2 \frac{A^2}{\sigma^2}}\right) \tag{5.17}$$

Previously, we proved that the optimum $\mathbf{w}$ is $\mathbf{w}_{opt} = \frac{\mathbf{h}^H}{\|\mathbf{h}\|}$. Therefore, after antenna selection, the optimum beamformer becomes

$$\tilde{\mathbf{w}_{opt}} = \frac{\tilde{\mathbf{h}}^H}{\|\tilde{\mathbf{h}}\|} \tag{5.18}$$

After substituting equation (5.18) into equation (5.17), we derive the minimum probability of error for the given fixed set of K selected antennas, which is equal to:

$$P_e = Q\left(\sqrt{2\|\tilde{\mathbf{h}}\|^2 \frac{A^2}{\sigma^2}}\right) \tag{5.19}$$

From the analysis above, we can conclude that the optimal set of selected antennas, which minimizes the probability of error, comprises the indices corresponding to the K largest (in magnitude) elements of the vector $\mathbf{h}$.

Chapter 6

MIMObit and CST

Neben's MIMObit is a software tool that models electromagnetic wave propagation under various types of environments in MIMO systems. It is appropriate to analyze MIMO systems and signal processing algorithms.

It is very important to mention that the data for both metallic and plasma antennas were extracted by using Microwave Studio, a software tool for designing, analyzing, and optimizing electromagnetic components and systems designed by Computer Simulation Technology **(CST)**.

Using MIMObit, we are able to model the systems introduced in Chapter 5. The produced channel coefficients vary according to distribution depending on the propagation environment and the antenna system used in MIMObit.

In this thesis, we simulate the communication between one transmitter and seven different receivers. The transmitter is equipped with one to four monopole antennas. while the receiver is equipped with a single one (MISO model system). The monopoles used are designed in MIMObit.

6.1 Basics Overview

Figure 6.1: MIMObit launch

The main goal of this section is to point out the parameters that need to be configured for MIMObit's functionality. First of all, by launching MIMObit the user is able to start a new project or load an existing one and continue some previous work(Fig.6.1). Five components must be defined in order to run a simulation in MIMObit :

Transmitter

This component refers to the transmitter's properties. First of all, it is essential to define the location in three-dimensional space (x, y, z), where x refers to the length, y refers to the width, and z to the height, all measured in meters m. In this project, the transmitter is centered in (0,0,3), meaning that it is centered in 0 lengths, 0 widths, with a given height of 3m. The Total Available Power is set to $30dBm$ with available bandwidth at $1MHz$. In Fig. 5.2, transmitter properties are illustrated.

Propagation enviroment

It is vital to analyze how the signal is transmitted through the environment. MIMObit offers two different propagation environments in order for the signal to reach the receiver, random and deterministic. Random means that random channel coefficients are produced every time we run a simulation. On the other hand, deterministic propagation environ-

ments produce the same channel coefficients. In our simulations, we use the deterministic ones and, more specifically, the **Line of Sight (LOS)**.

Receiver

The receiver has similar properties to those of the transmitter. The location follows the same notation (x, y, z) and defers based on which antenna is used. Nevertheless, the receiver remains $100m$ away from the transmitter antenna with a given height of $3m$. Furthermore, there are some properties for gain, resolution, and bandwidth(Fig.7.10).

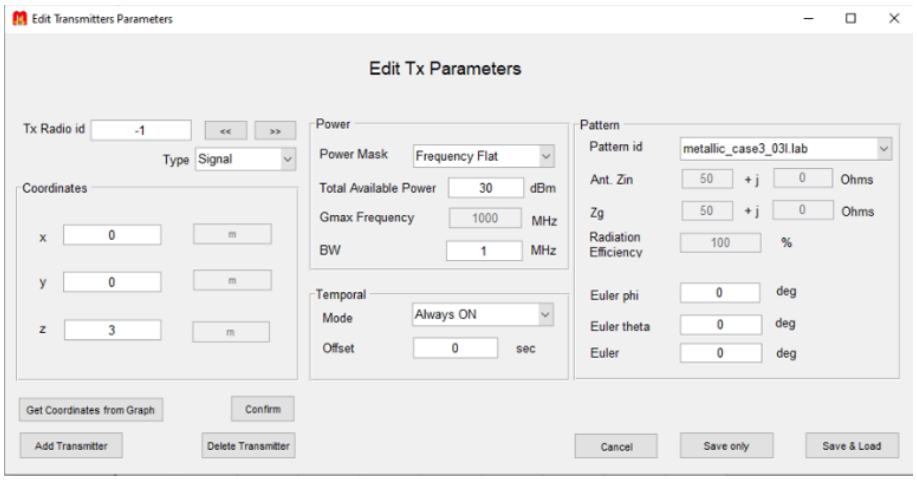

Figure 6.2: Transmitter setup

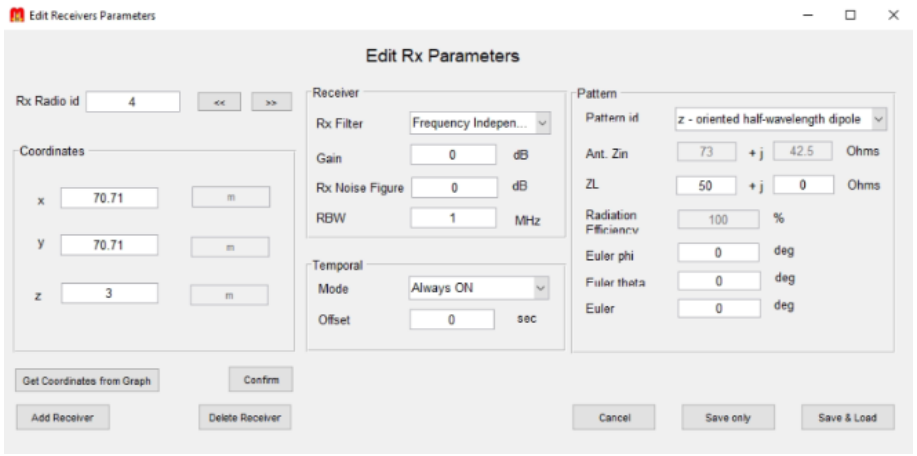

Figure 6.3: Receiver setup

Frequency

This component refers to the frequencies at which our system works(Fig. 5.4). In our case, we use the bandwidth between 400MHz and 800MHz with a 100Mhz step. We emphasize at 500Mhz-650Mhz with 10Mhz step.

Time

This component refers to the user's ability to modify the temporal behavior of any T_x or R_x radio. We used the value 0 for our simulations, as seen in Fig. 6.4.

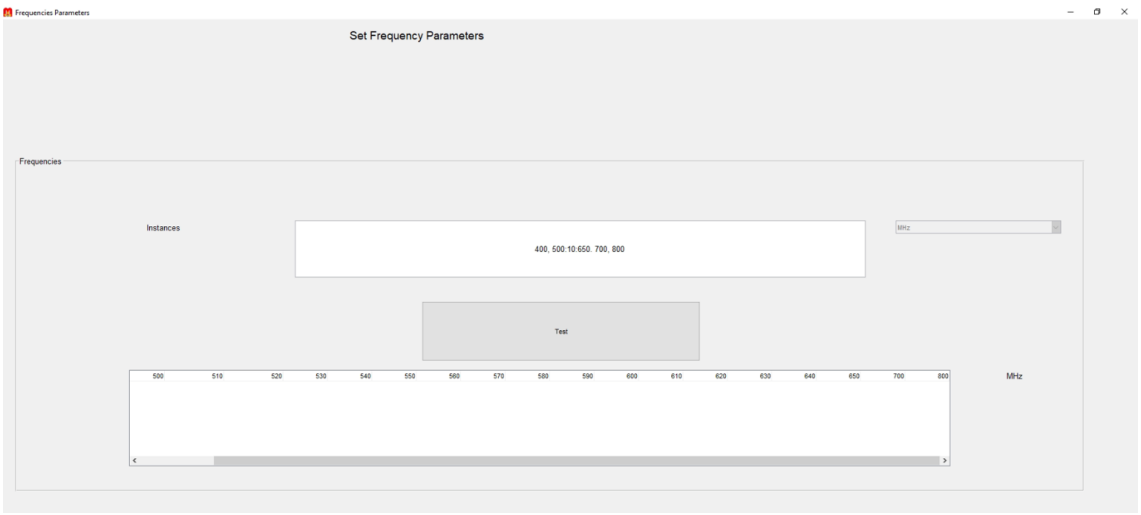

Figure 6.4: Frequency setup

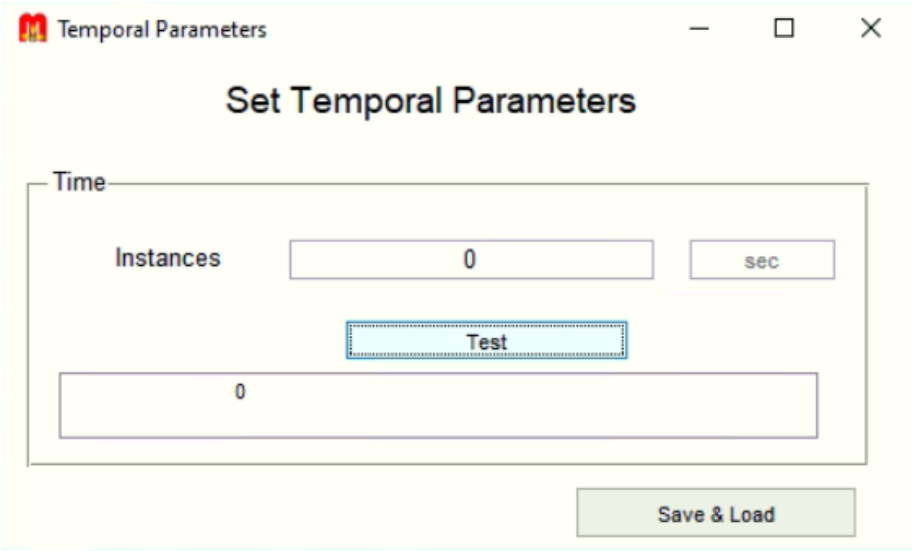

Figure 6.5: Time setup

6.2 Setup

In our experiments, seven antennas were used to draw results. As illustrated in Fig 6.6, the setup consists of seven receiver antennas from 0°(R_{x1}) to 90°(R_{x7}) with a 15°step between the receiver antennas.

After finishing the setup for all the cases evaluated, we are moving forward with the implementation of each receiver antenna separately. For instance, Fig. 6.7 depicts the user interface for case 4, where R_{x4} is tested. It is essential to mention that this process is repeated for all seven cases.

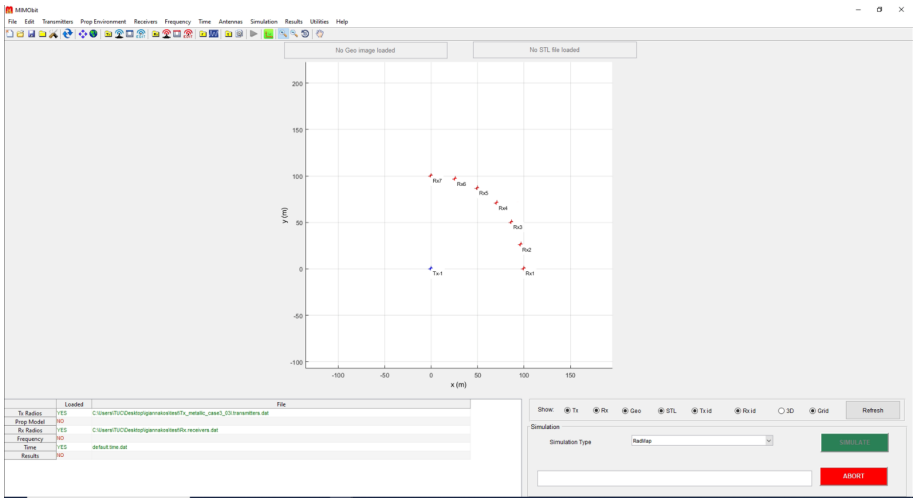

Figure 6.6: User interface for all cases

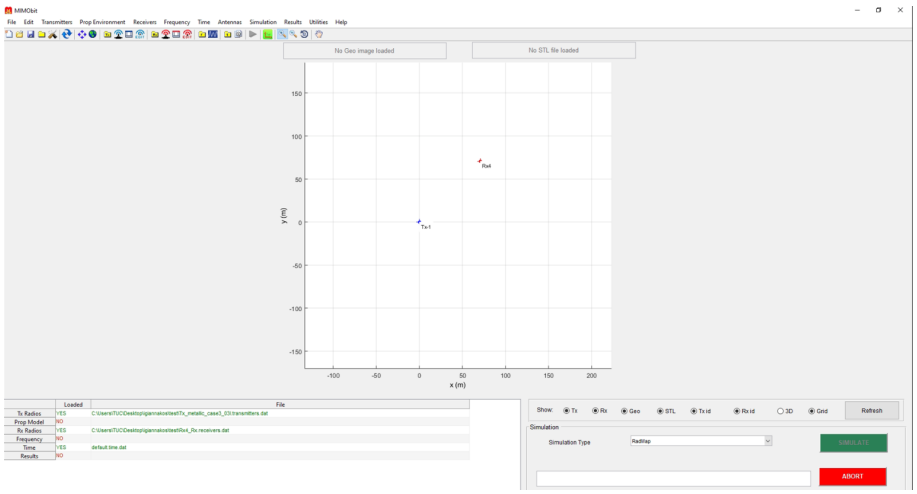

Figure 6.7: User interface for case 4

After finishing an experiment in MIMObit, a .dat file is produced, which contains the final results and can be seen below (Fig 6.8).

It is undeniable that after the experiment in MIMObit is finished, a .dat file is produced, which contains all the vital information needed. More particularly, as illustrated in Fig. 6.8, the MIMObit returns the channel coefficients for both real and imaginary parts for every frequency. Furthermore, it is crucial to clarify that as far as the transmitter is concerned, information about every port is recovered separately. For example, we can see that for the same receiver antenna, we are getting two different lines of information for the same frequency, one for the first port and one for the second.

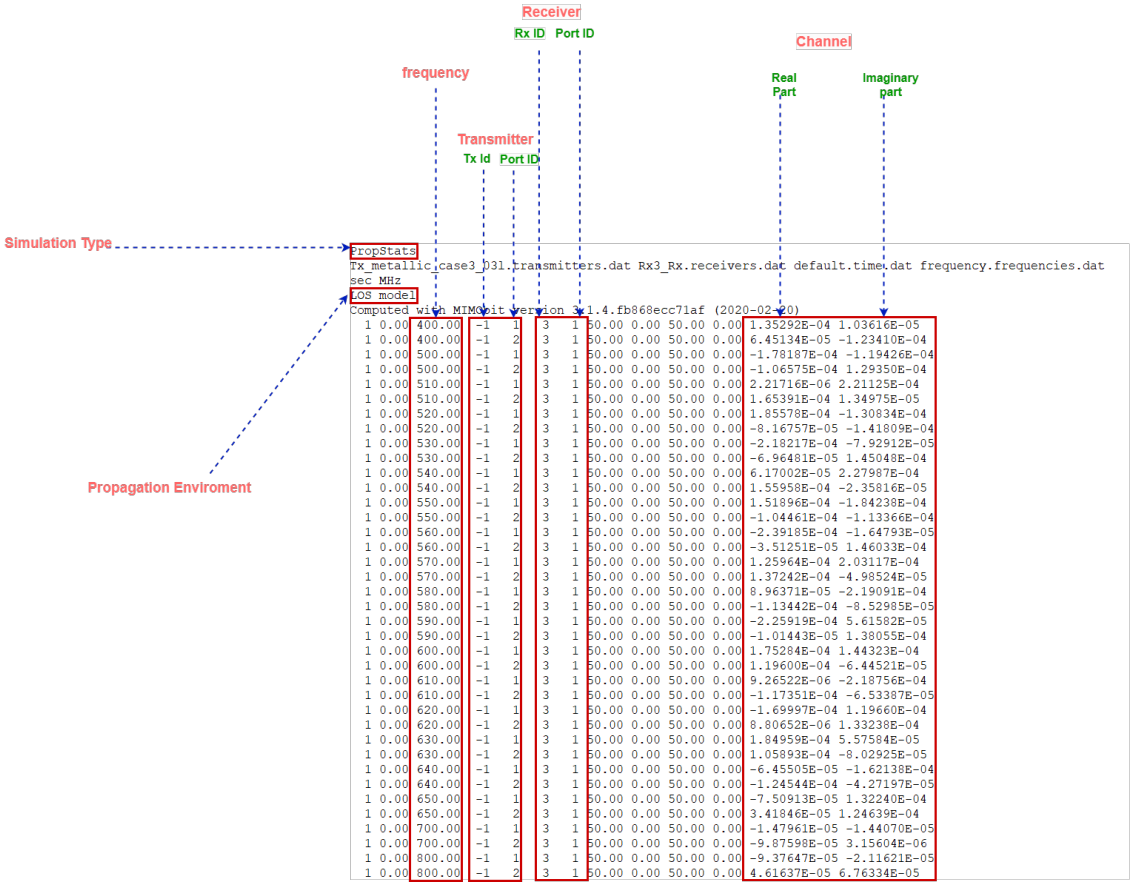

Figure 6.8: .dat file

Chapter 7

Experiments

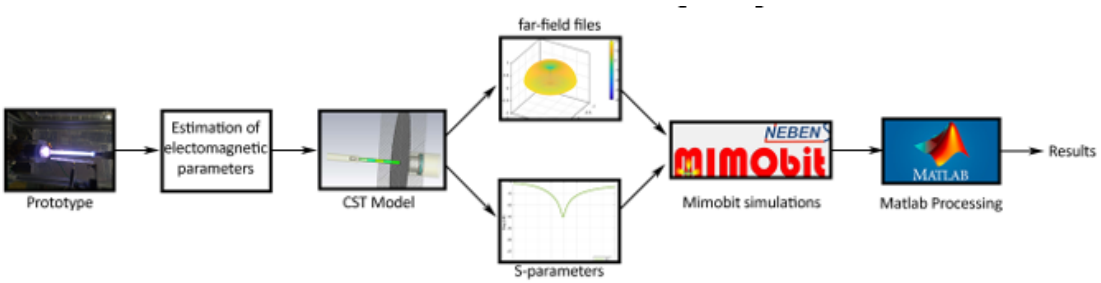

Figure 7.1: Experimental process for monopoles

In this final Chapter, we will present the experiments made to complete this Thesis. Although the theory has a significant role, experiments will prove our statements and allow us to look deeper into the antennas, their properties, and the differences between plasma and metallic ones.

In Fig. 7.1, the experimental process is illustrated step by step. Firstly, electromagnetic parameters were estimated from the prototype antenna, which was then used to create the CST model with radiation patterns and S-parameters. After that, the CST model was introduced to the MIMObit application to experiment in the MIMObit environment. To be more precise, CST files include all the antenna characteristics (both for metallic and plasma) needed to complete the investigation. Finally, after MIMObit files are produced, they are imported into MATLAB to be processed. Every .dat file (files produced after MIMObit) was read properly and extensively. After that, it was a lot easier to extract the data and process them correctly to draw results and create useful graphs that would be handed over on the following pages.

7.1 Experiment Description

For the experiments, a transmitter antenna is located in the center of the axes with coordinates (0m,0m,3m) where z=3m is the height, and it is standard for all the antennas.

Seven receiver antennas are located at a 100m distance from the transmitter, every 15°. For example, the first receiver is located at (100m,0m,3m), at 0°with the transmitter, while the second receiver is at (96.59m,25.89m,3m), at a 15°with the transmitter. Thus, there will be seven different cases from 0°to 90°(0°,15°,30°,45°,60°,75°,90°). Further, it is essential to mention that there is no need to test other degrees over 90°because they will be similar due to symmetry.

As far as frequencies are concerned, they are a constant array from 400MHz to 800Mhz with a given step of 100MHz, except from the frequencies 500:650, where a step of 10MHz is used to draw more accurate results.

For the propagation model, Line Of Sight (LOS) is used.

Antenna properties

For the **metallic antennas**, a metallic monopole was used with a length of l=11.875cm. The transmitter is a Quadruple metallic antenna with total available power of 30dBm and a bandwidth of 1MHz. On the other hand, the receiver is a z-oriented half-wavelength metallic dipole, while the Resonance frequency is set at f $\simeq$ 598MHz (λ=50.132518cm).

On the contrary, for the **plasma antennas**, a high-density plasma monopole was used with a length of l=10cm. The transmitter is a Quadruple plasma antenna with total available power of 30dBm and bandwidth of 1MHz. The receiver antenna is a z-oriented half-wavelength metallic dipole, while the Resonance frequency is set at f $\simeq$ 598MHz (λ=50.132518cm).

7.2 Channel Power

In the first part of the experiments, we will perform antenna selection for all of the four monopoles consisting of the antenna for d=12(0.24λ), 16(0.32λ), 20(0.4λ), 24cm(0.48λ) where d is the distance between the monopoles. We plot the channel power $\|H\|^2$ over the frequency array for all the cases that arise. Channel power can be calculated as follows:

$$\|h\|^2 = \sum_{n=1}^{n} |h|^2$$

where n=4 is the number of the monopoles. In fact, the channel power of each radiating monopole is added to find the total one.

In the figure below, the available cases for the antenna selection can be seen:

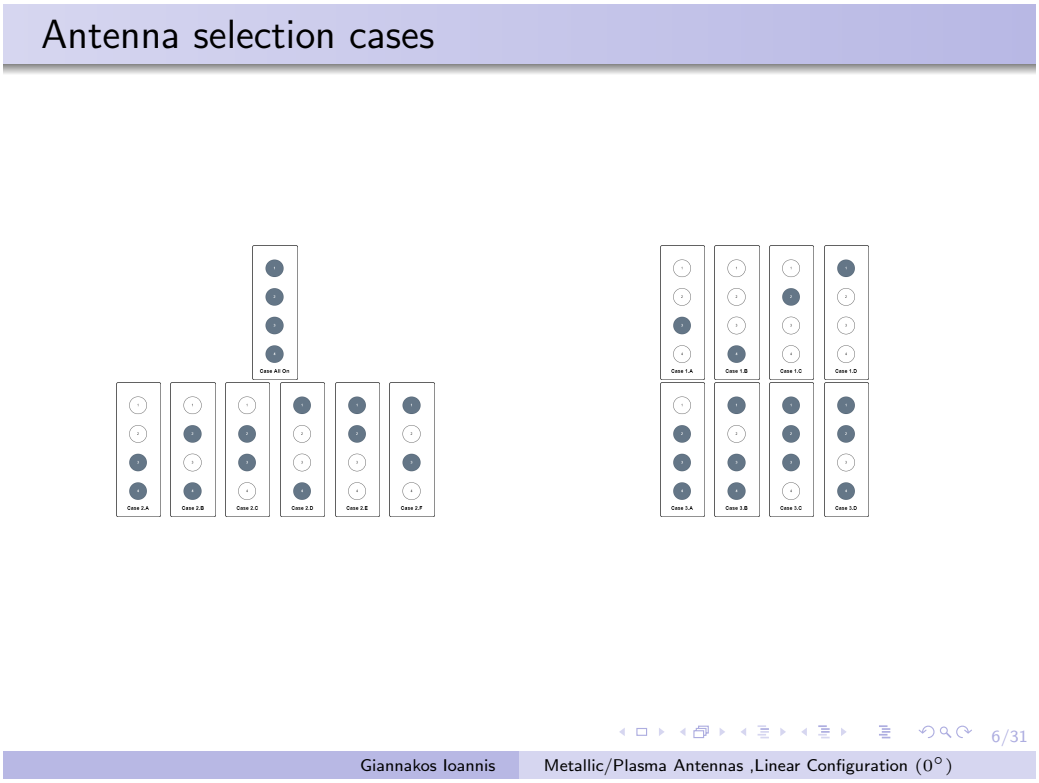

Furthermore, we will examine actual channel power, and finally, we will inspect and compare achievable and conventional graphs.

We will perform all of the experiments mentioned above for both metallic and plasma antennas in order to make a safe assumption about the plasma ones and their fundamental differences from metallic ones.

In the subsequent pages, we will present a graphical presentation for some experiments. To be more precise, experiments for 0°,45°, and 90°will be presented in order to analyze

and comment on the results.

Metallic/Plasma Antennas 30°

Simulation Properties (2)

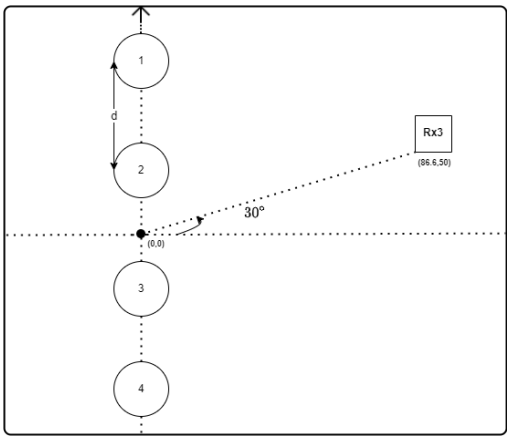

Simulations for $d = 12,\ 16,\ 20,\ 24$cm.

In the first case, we perform our experiment on a receiver antenna located at x=86.6m, y=50m, and height z=3m and at 30°with the transmitter, which is located at x=0m, y=0m, and height z=3m, as can be seen in the figure above. The simulations will be for four distances d=12cm, 16cm, 20cm, and 24cm. Firstly, we will work on antenna selection for all the cases (all monopoles radiating, one monopole radiating, two monopoles radiating, and three monopoles radiating).

Our objective is to compare metallic and plasma antennas through various experiments and graphical simulations that we will analyze on the following pages for this particular case.

Channel power for different values of d.

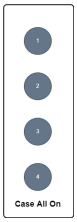

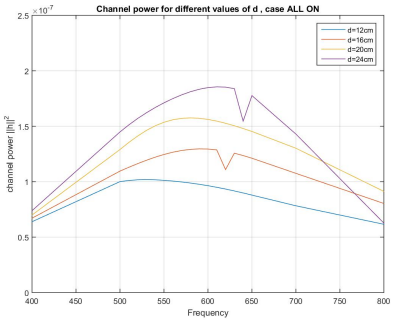

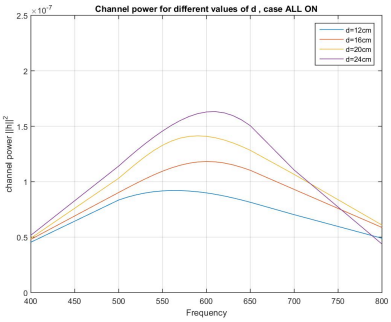

Channel power for different values of d. Case 1.A/1.B

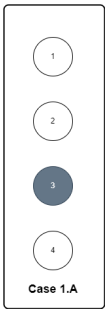

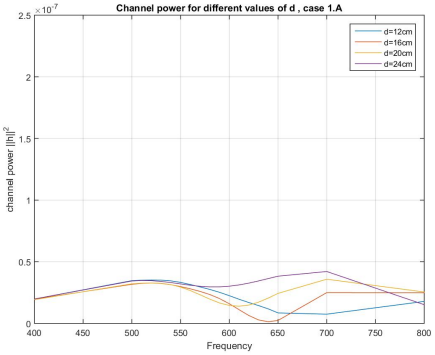

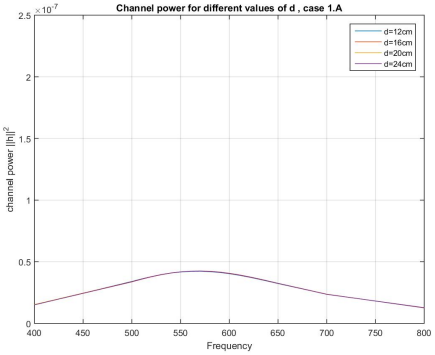

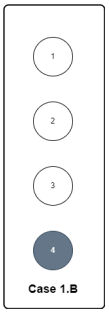

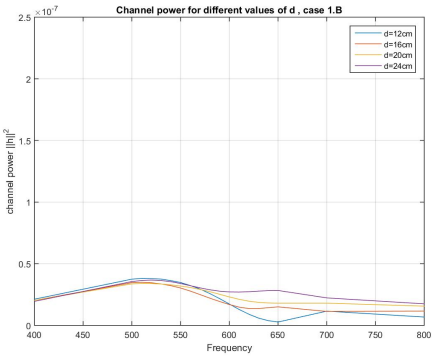

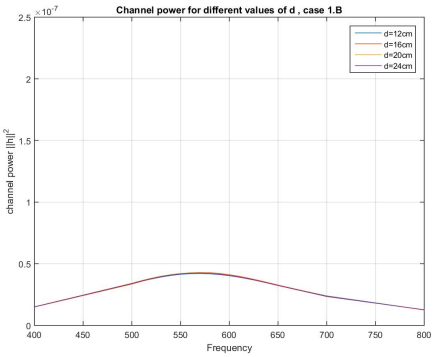

Channel power for different values of d.. Case 1.C/1.D

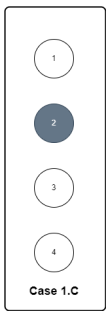

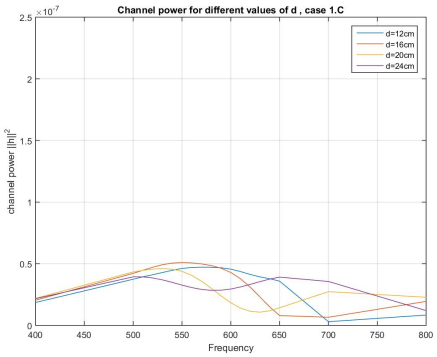

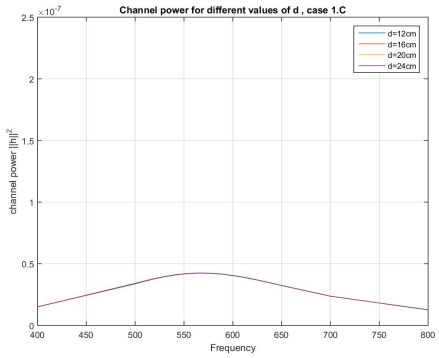

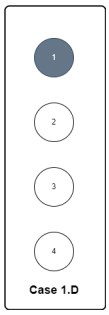

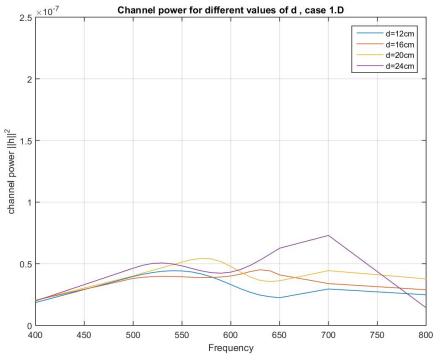

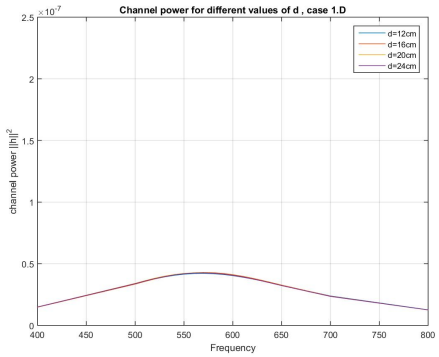

Channel power for different values of d. Case 2.A/2.B

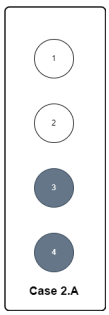

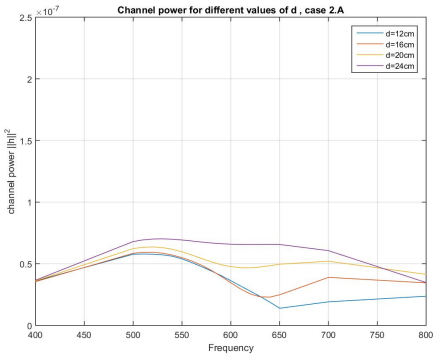

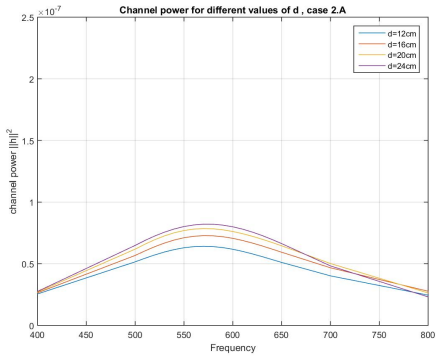

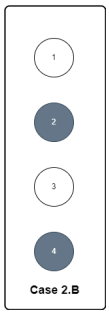

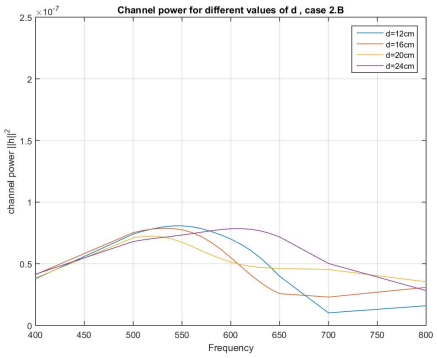

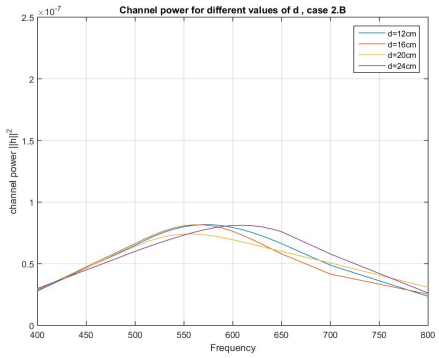

Channel power for different values of d. Case 2.C/2.D

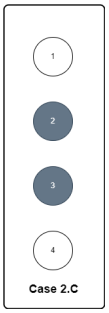

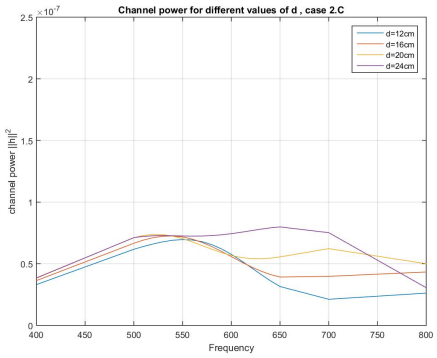

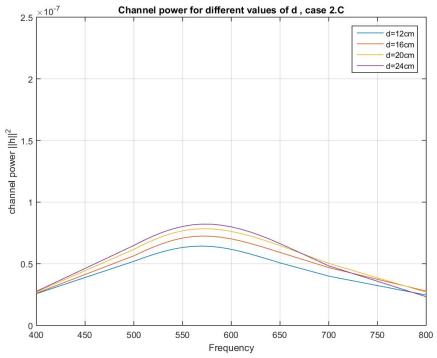

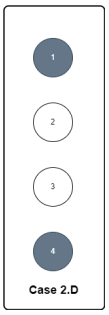

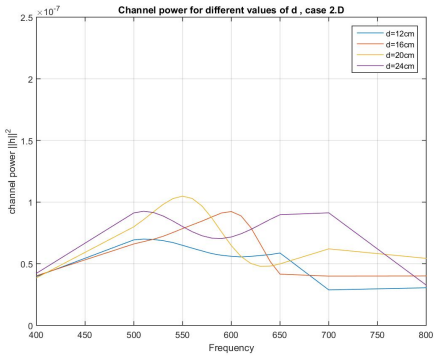

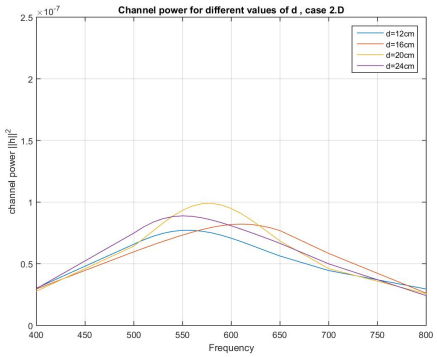

Channel power for different values of d. Case 2.E/2.F

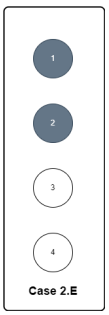

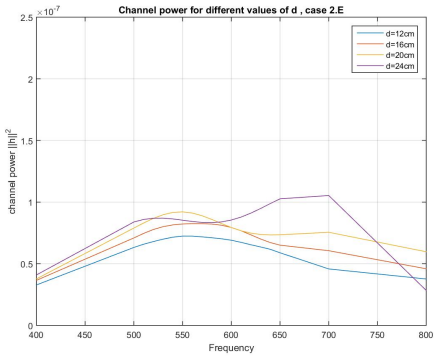

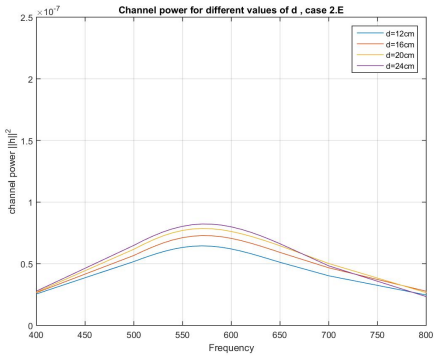

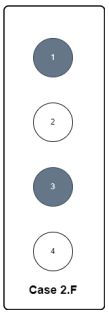

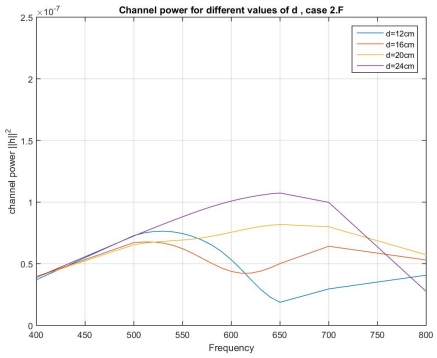

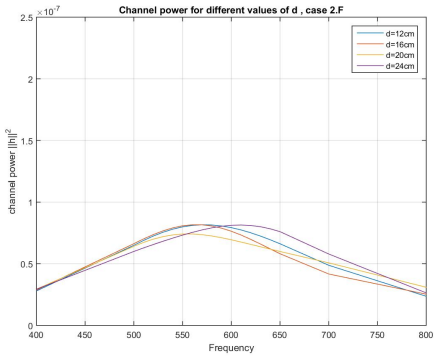

Channel power for different values of d.. Case 3.A/3.B

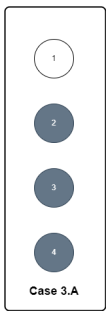

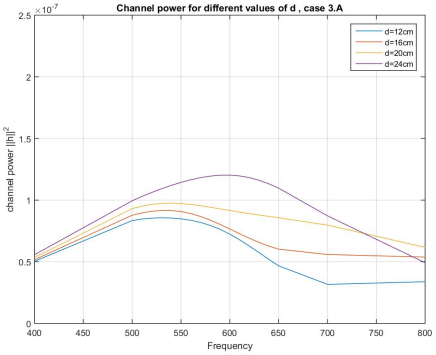

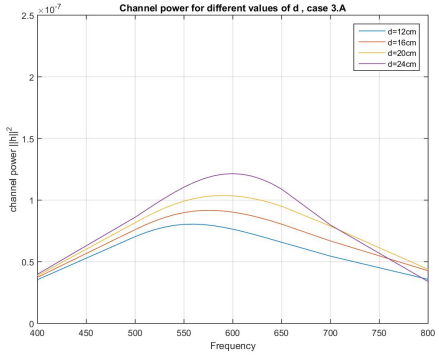

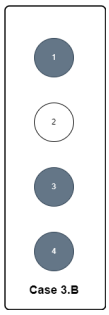

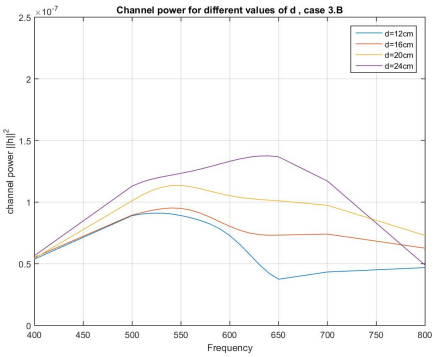

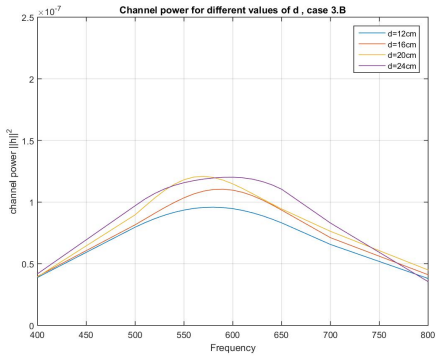

Channel power for different values of d. Case 3.C/3.D

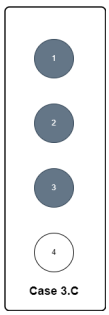

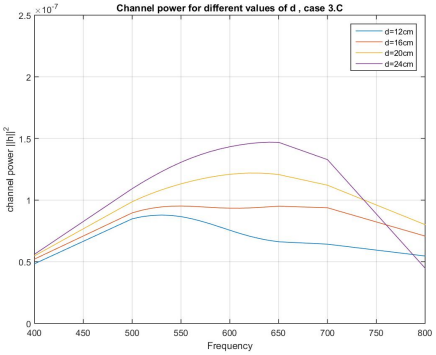

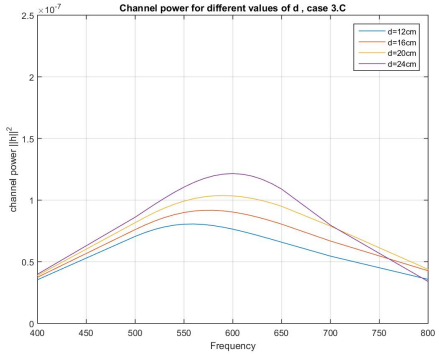

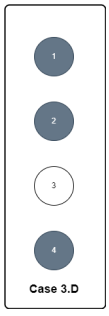

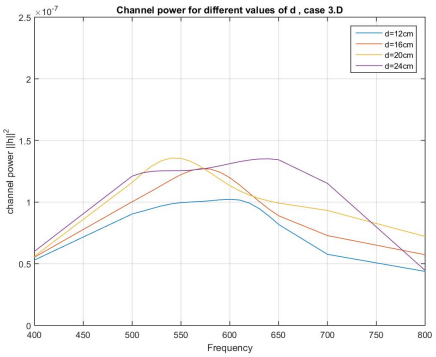

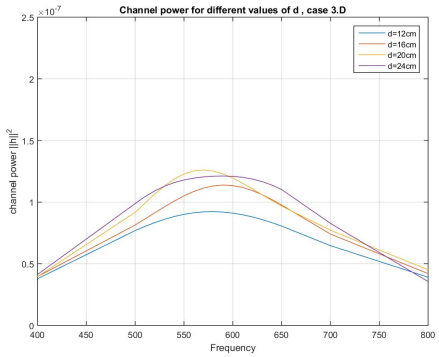

The above graphical simulations show how the channel power $\|H\|^2$ is plotted over frequencies for all the cases after attempting antenna selection. The first thing we monitor is the plasma plots' smoothness and similarity. The channel power of the metallic antenna appears to be harsher, with many spikes and angles.

Initially, in the presence of a single radiating monopole, the metallic antennas exhibit minimal dissimilarities. Notably, their spatial initiation and termination points remain remarkably consistent. However, the introduction of additional monopoles (two, three, and the collective activation of all) ushers in discernible disparities among the antennas. Correspondingly, in the case of a singular monopole, the plotted responses at varying distances demonstrate a high degree of resemblance. Nevertheless, as we transition to the subsequent scenarios, the plots evince more pronounced divergences, though not of a significantly substantial nature. The intriguing observation emerges when all monopoles are concurrently activated, leading to a distinct tendency of the plots to repel each other.

Further, it is crucial to mention that in the study case where two monopoles are on, we observe that for both metallic and plasma antennas, when nearby monopoles are radiating, the plots appear more precise and smoother with little or no mutual points. Conversely, when the monopoles are not neighboring, they produce steep and fluctuating graphical properties. This observation also applies to the last case with the three monopoles switched on. The Fig. 7.2 below is a clear example of this note.

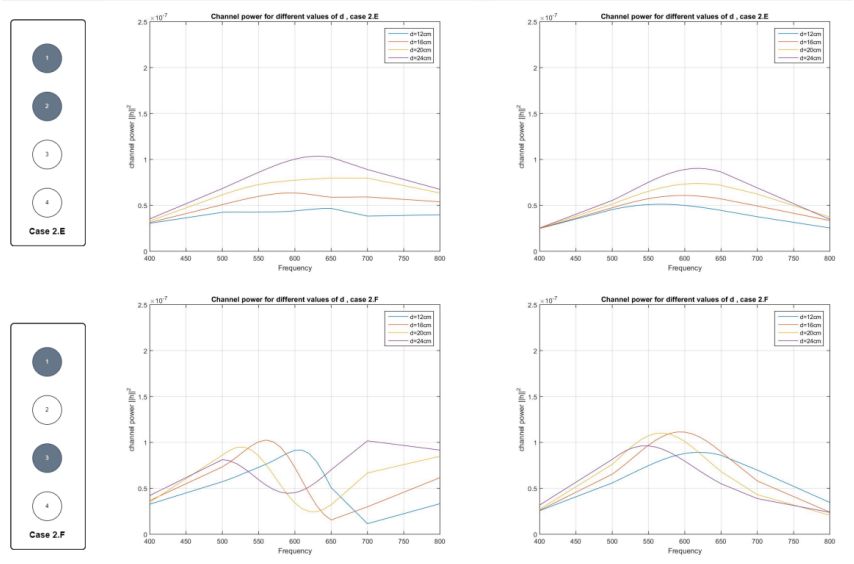

Figure 7.2: Difference between nearby and not neighboring monopoles

So, we can conclude that spacing between the radiating monopoles creates uncertainty in the channel power estimation.

Comparison of $\|H\|^2$ for d=20cm

Comparison of $\|H\|^2$, 1 port selected, $d = 20$cm (0.4λ).

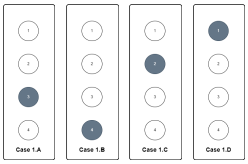

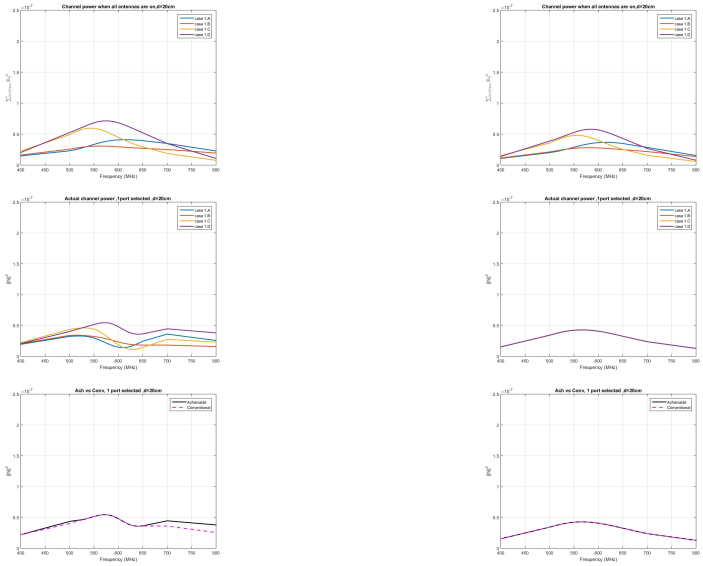

Comparison of $\|H\|^2$, 2 ports selected, $d = 20$cm (0.4λ).

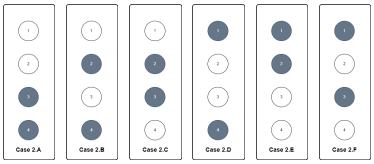

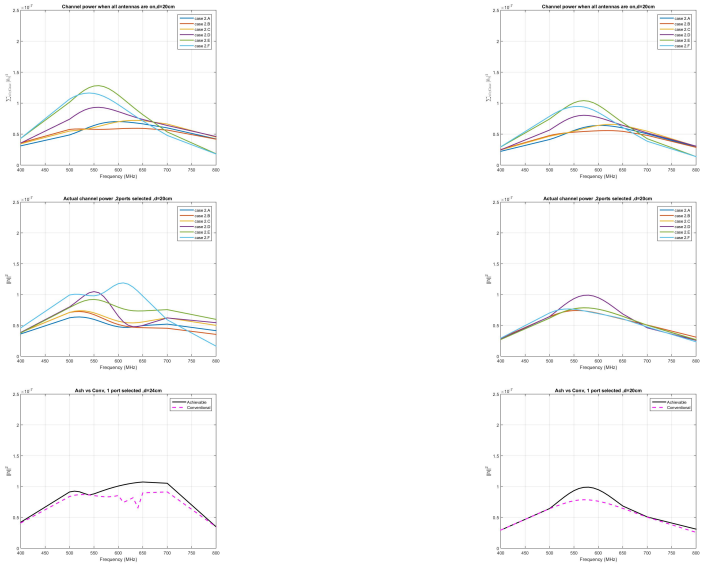

Comparison of $\|H\|^2$, 3 ports selected, $d = 20$cm (0.4λ).

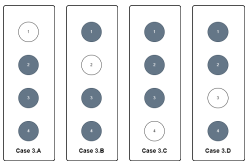

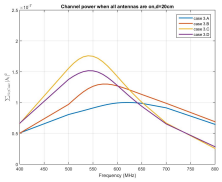
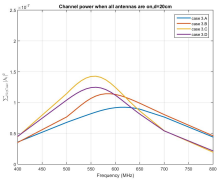
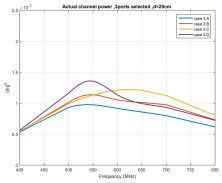
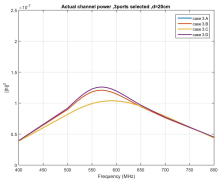
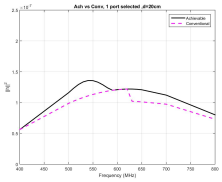
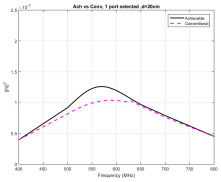

In the above experiments, we produce three different graphical simulations for both metallic and plasma cases:

- Channel power when all antennas are on
- Actual channel power
- Achievable vs. Conventional

Regarding **Channel power when all antennas are on**, we utilize the case where all monopoles radiate and then perform antenna selection. For example, in the first study case where only one monopole is radiating, we use the data from the all-on case and calculate only the channel power of the one monopole we want. Then, we apply the same technique to the rest cases and plot them in the same graphical simulation. We work similarly for the rest study cases(two monopoles radiating, three monopoles radiating).

Continuing on, in the **Actual channel power** simulations, we conduct antenna selection separately for each case. For instance, in the first scenario involving only one radiating monopole, we plot the channel power for all four different antenna selection cases within the same graphical representation. The distinction from the previous simulation lies in the "Channel power when all antennas are on," where antenna selection is performed with all the monopoles activated simultaneously.

It is essential to emphasize that Mutual Coupling significantly impacts the channel power, as the radiating monopoles' performance directly influences one another. This coupling effect can lead to variations in the channel power values, affecting the overall antenna system's performance. Hence, in the simulations where all antennas are active, we need to consider the interactions between them, as it plays a crucial role in determining the actual channel power distribution across different degrees.

In the last graphical simulation, we observe the presentation of two plots: **Achievable** and **Conventional**. **Achievable** plot illustrates an antenna's ideal or theoretical radiation characteristics. Specifically, it depicts the total maximum of the **"actual channel power plot"**.
Conversely, the **Conventional** plot portrays the actual performance of the antenna. To generate the **Conventional** plot, we analyze the **"Channel power when all antennas are on"** scheme and identify the highest points across all plots. Subsequently, we refer to the **"actual channel power"** plot and depict the plot that exhibits the highest value at the **"Channel power when all antennas are on"**. This can be observed in Figure 7.3 as an example.

Additionally, it is crucial to highlight an observation. On slide 26, we observe that for metallic antennas at a distance of $d = 20cm$, the Conventional plot does not attain the Achievable plot. This indicates that the actual performance of the antenna will not achieve the ideal transmission across any of the studied frequencies. Conversely, for plasma

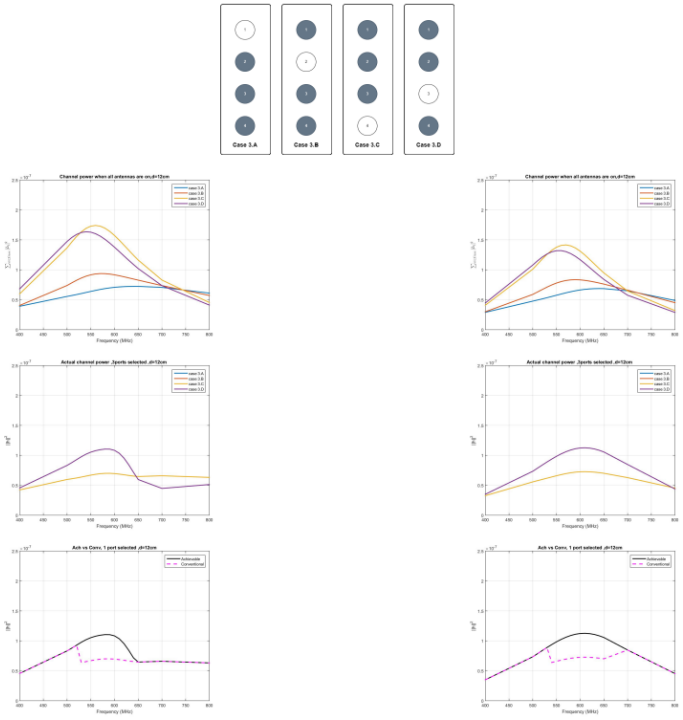

Figure 7.3: Example

antennas under the same conditions, we observe that the Conventional plot aligns with the Achievable plot after reaching 650MHz.
Nevertheless, in the majority of cases, the Conventional plot closely approaches or aligns with the Achievable plot across the widest range of frequencies.

Metallic/Plasma Antennas 45°

Simulation Properties (2)

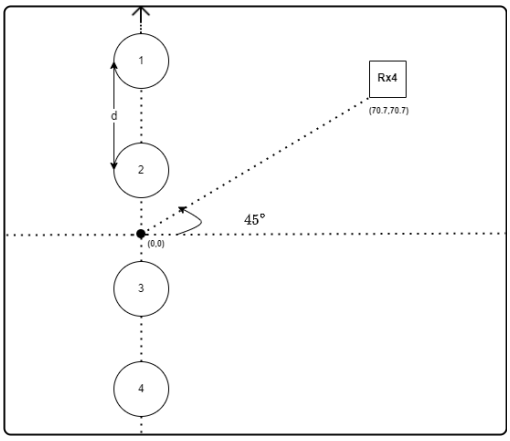

Simulations for $d = 12,\ 16,\ 20,\ 24$cm.

In the second experiment set, we perform our experiment on a receiver antenna located at x=70.7m, y=70.7m, and height z=3m and at 45°with the transmitter, which is located at x=0m, y=0m, and height z=3m, as can be seen in the figure above. The simulations will be for four distances d=12cm, 16cm, 20cm, and 24cm. Firstly, we will work on antenna selection for all the cases (all monopoles radiating, one monopole radiating, two monopoles radiating, and three monopoles radiating).

Our objective is to compare metallic and plasma antennas through various experiments and graphical simulations that we will analyze on the following pages for this particular case.

Channel power for different values of d.

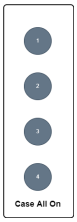

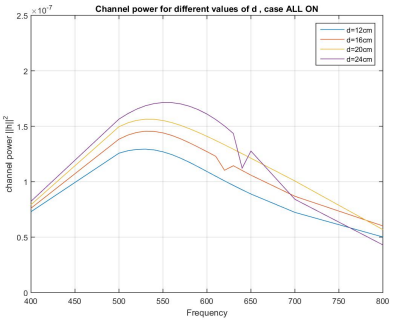

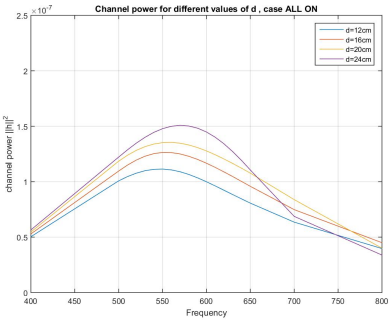

Channel power for different values of d. Case 1.A/1.B

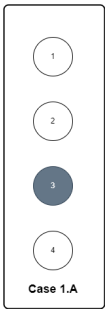

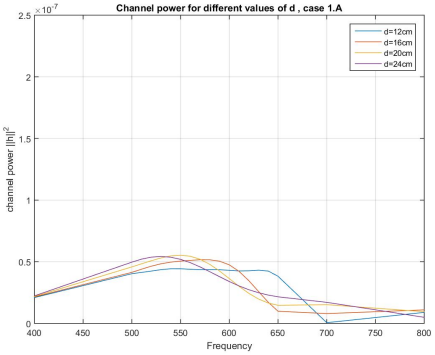

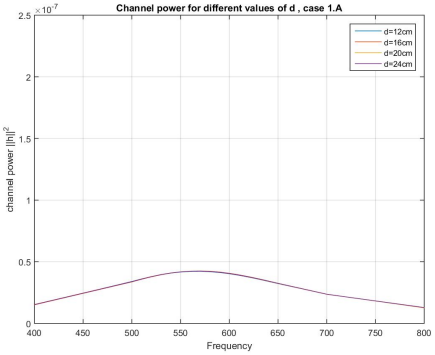

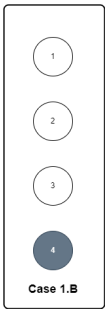

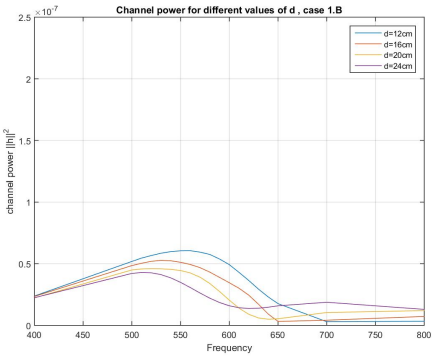

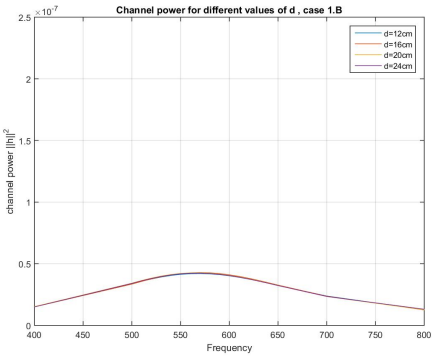

Channel power for different values of d. Case 1.C/1.D

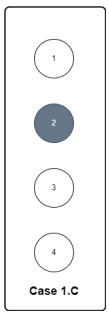

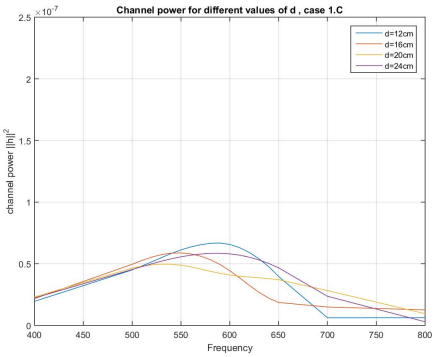

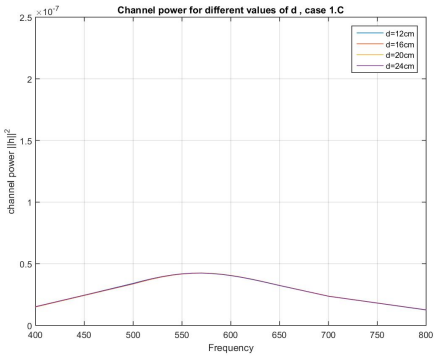

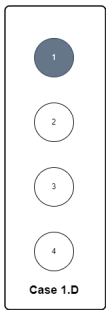

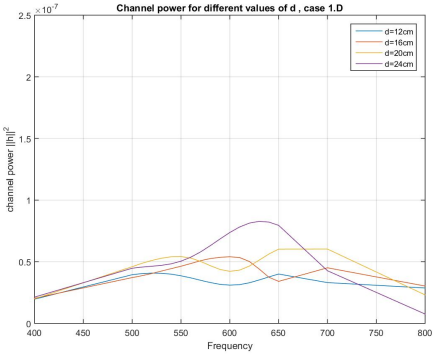

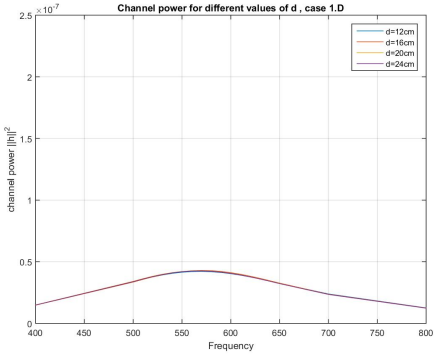

Channel power for different values of d. Case 2.A/2.B

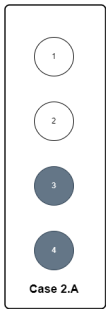

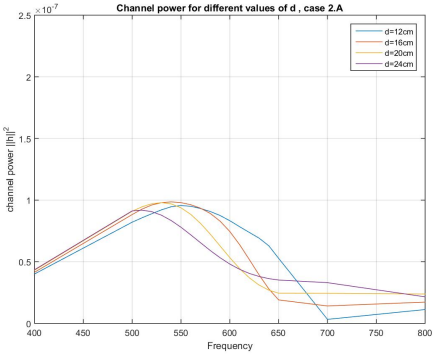

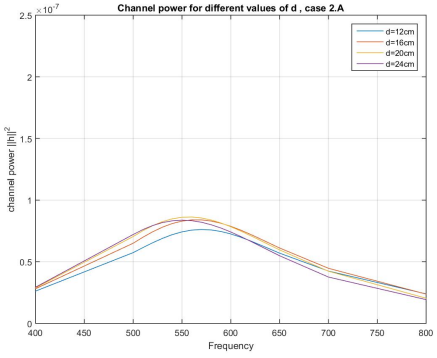

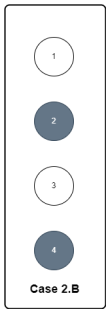

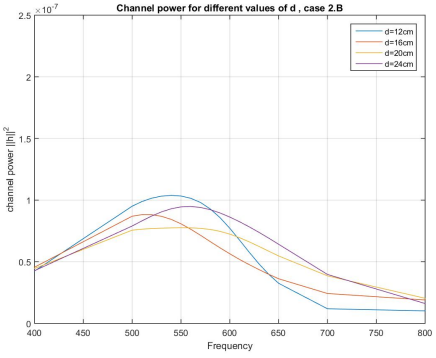

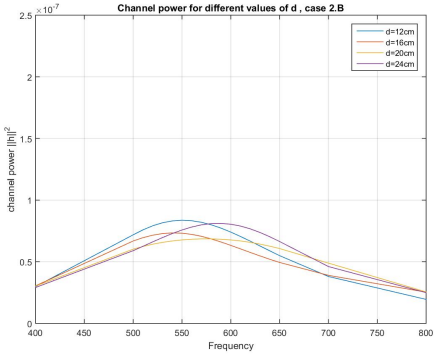

Channel power for different values of d. Case 2.C/2.D

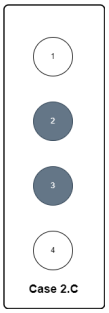

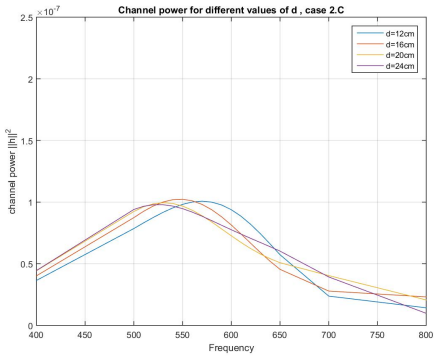

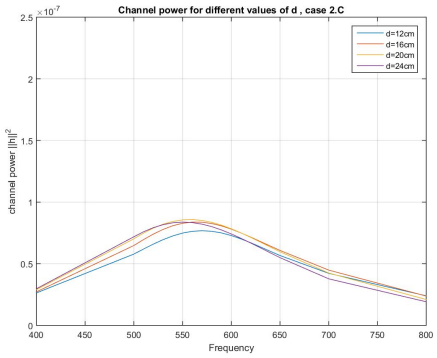

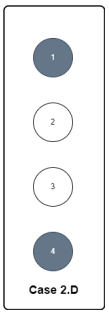

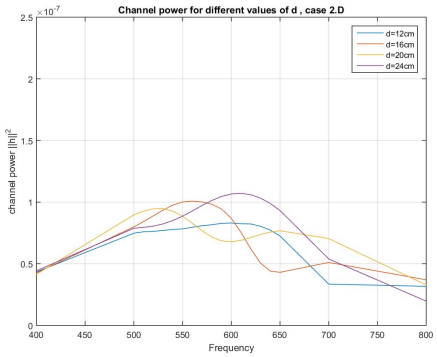

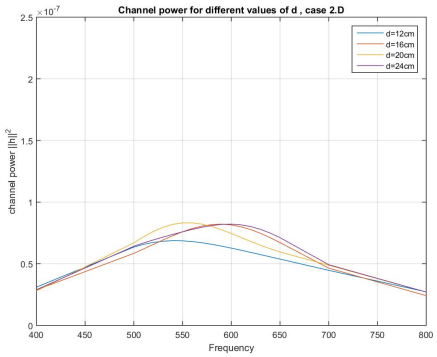

Channel power for different values of d. Case 2.E/2.F

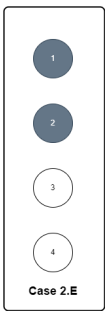

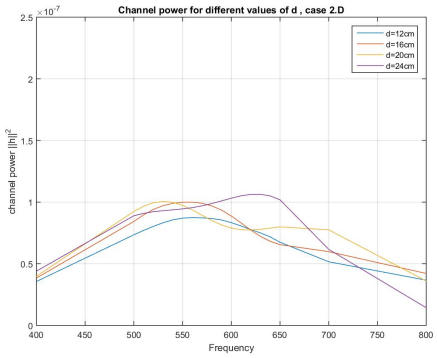

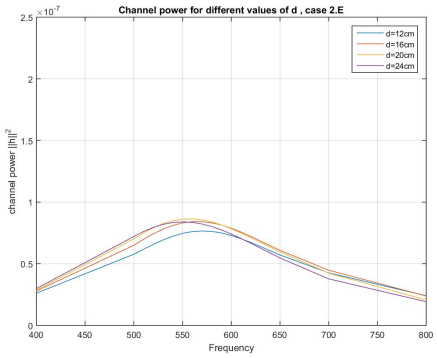

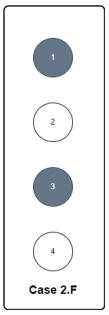

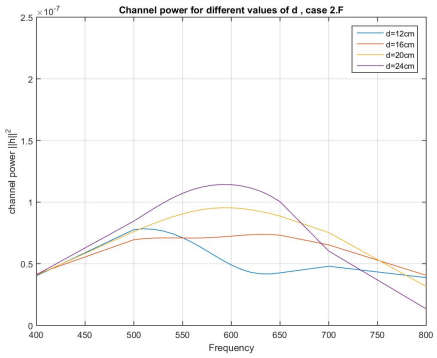

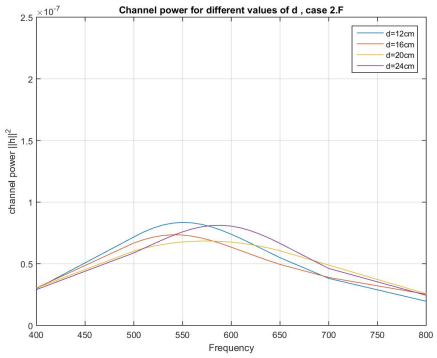

Channel power for different values of d.. Case 3.A/3.B

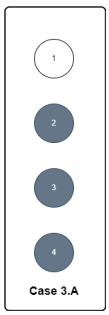

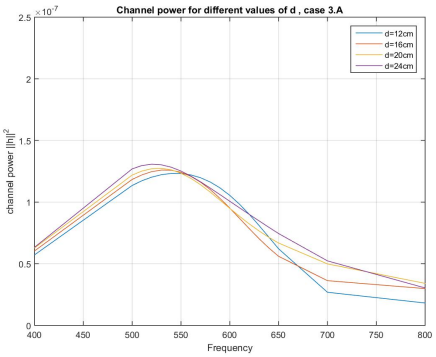

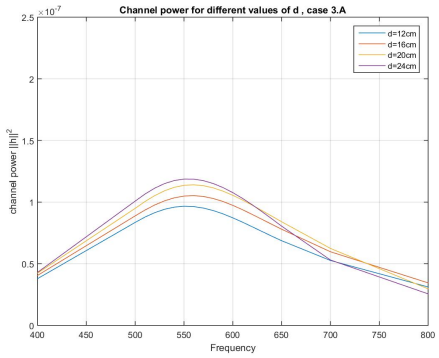

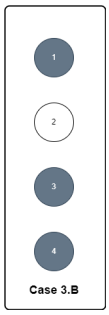

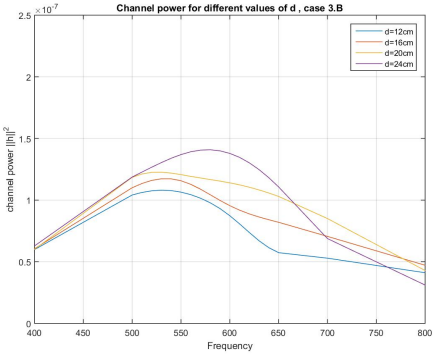

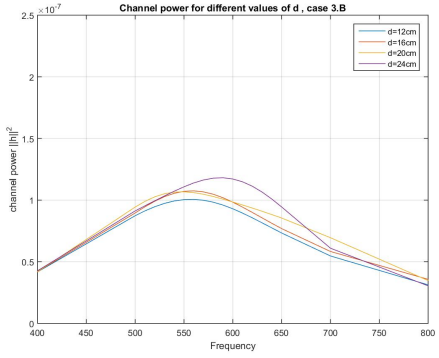

Channel power for different values of d. Case 3.C/3.D

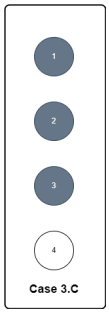

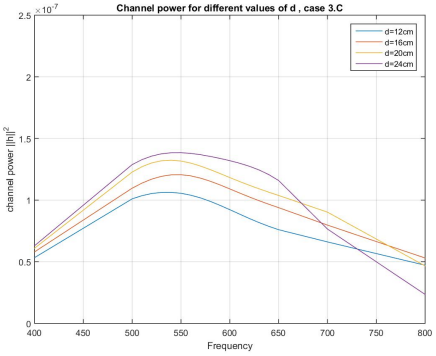

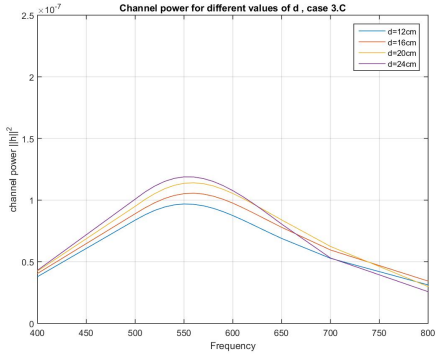

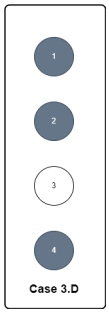

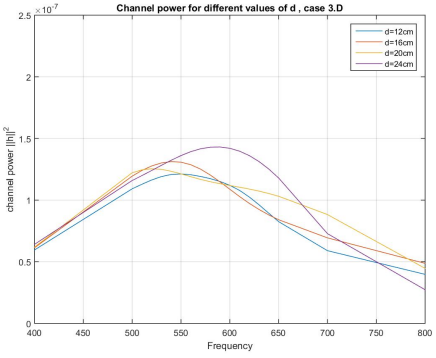

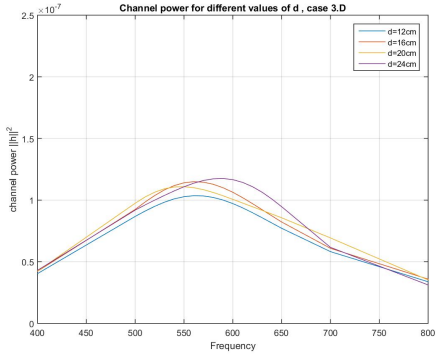

The aforementioned graphical simulations exhibit the plotting of the channel power $|H|^2$ across frequencies for all cases following antenna selection attempts.
Many of the observations made in the context of the **30°** case also hold for the **45°** case. Our focus will be directed towards identifying the disparities and resemblances between these two scenarios, allowing us to discern the impact of receiver angle variations on transmitter antennas.

Conversely, with the 30°case, 45°appears to have minor sensitivity for frequencies over 600MHz. Moreover, it is notable that both cases demonstrate their peak values within the range of 500MHz to 600MHz, irrespective of the cases and distances considered.
Examining case 3, we note that the simulations exhibit minimal variations and maintain close proximity to one another, proving that regardless of distance, the plots are similar for both metallic and plasma antennas.

For example, in Fig. 7.4, we can see that case 3's four different plots are close to each other. Furthermore, the highest point is in the frequency range between 500MHz-550MHz, and last but not least, we can observe that after 600Mhz, the plots decline, meaning that the channel power is falling.

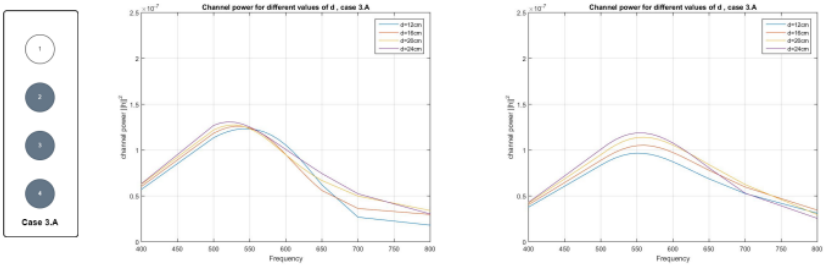

Figure 7.4: Case 3 for 45°experiment

Comparison of $\|H\|^2$ for d=20cm

Comparison of $\|\mathbf{H}\|^2$, 1 port selected, $d = 20\text{cm}$ (0.4λ).

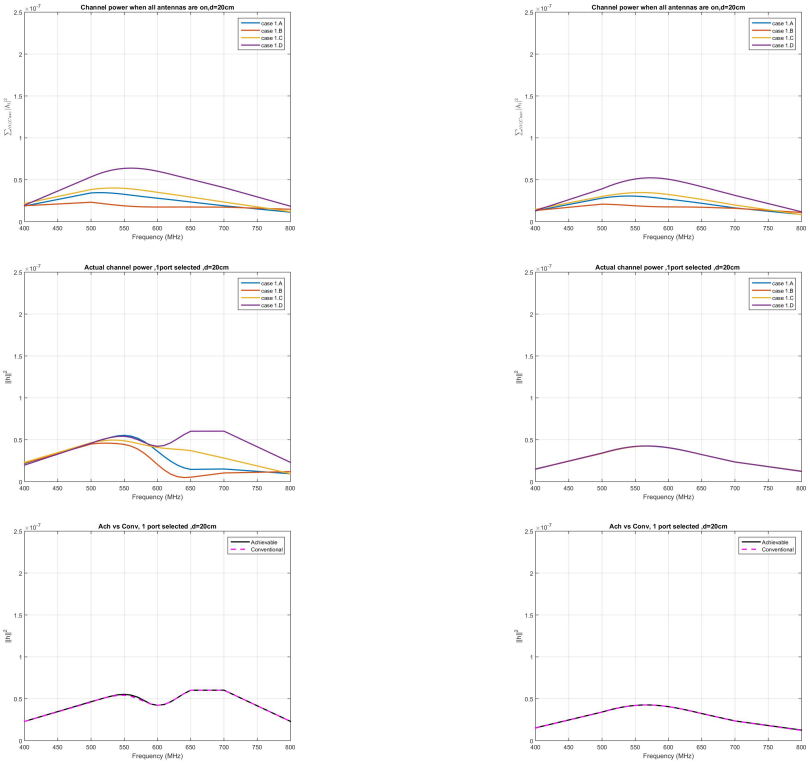

Comparison of $\|\mathbf{H}\|^2$, 2 ports selected, $d = 20\text{cm}$ (0.4λ).

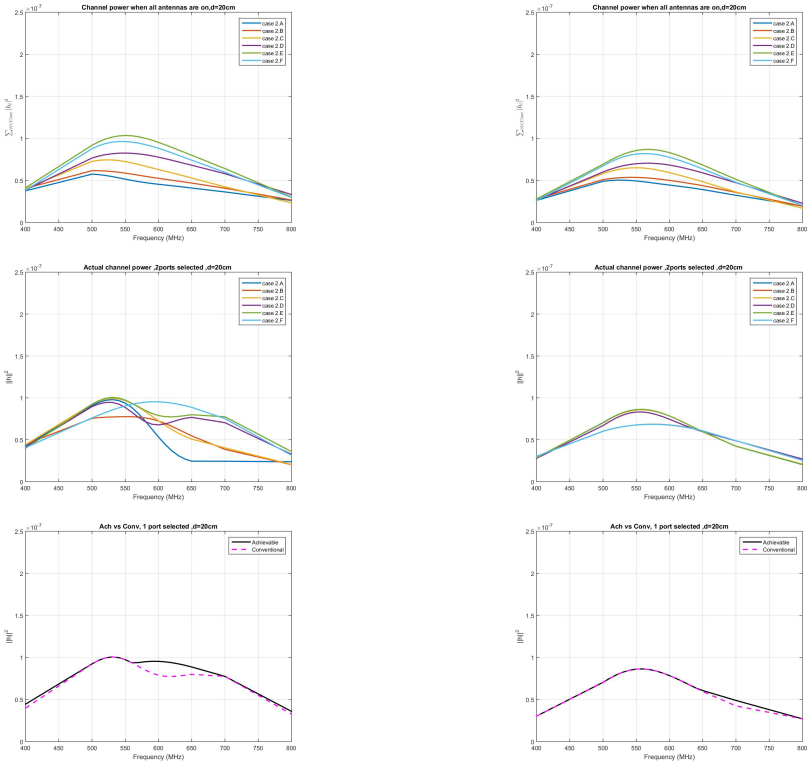

Comparison of $\|\mathbf{H}\|^2$, 3 ports selected, $d = 20$cm (0.4λ).

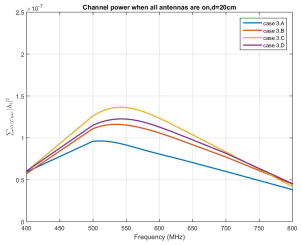

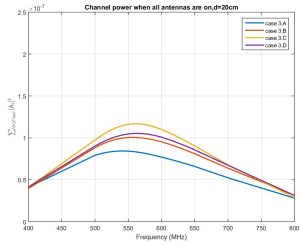

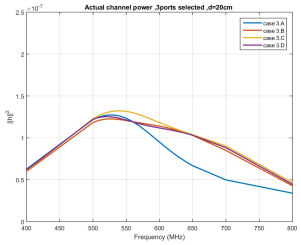

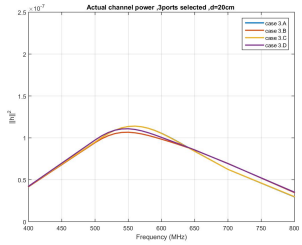

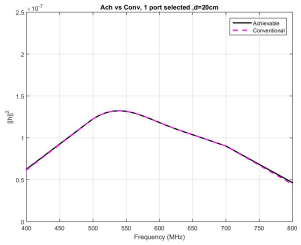

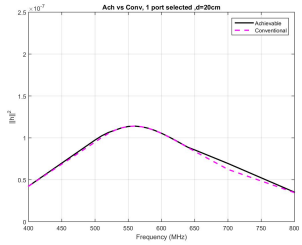

In the above experiments, we produce three different graphical simulations for both metallic and plasma cases:

- Channel power when all antennas are on
- Actual channel power
- Achievable vs. Conventional

The initial observation in this section revolves around the number of plots presented in the "Actual channel power" graph. In order to analyze this observation to a higher extend we will need the experiment result from the 0°case. In the 0° case (case where only one monopole is radiating), we observe the generation of two plots among the available four cases. Conversely, in the 45° case, there are four plots. This occurrence can be attributed to the symmetry of monopoles in the 0° case, producing identical plots. In contrast, the absence of symmetry in the 45° case leads to distinct plots. The same observation holds for the remaining two cases (two monopoles on, three monopoles on). Notably, in the case of two monopoles transmitting at a 45° angle, the "Actual channel power" graphical simulation produces six plots instead of the four observed in the 0° case.
In the Fig. 7.5 we can clearly see the above observation.

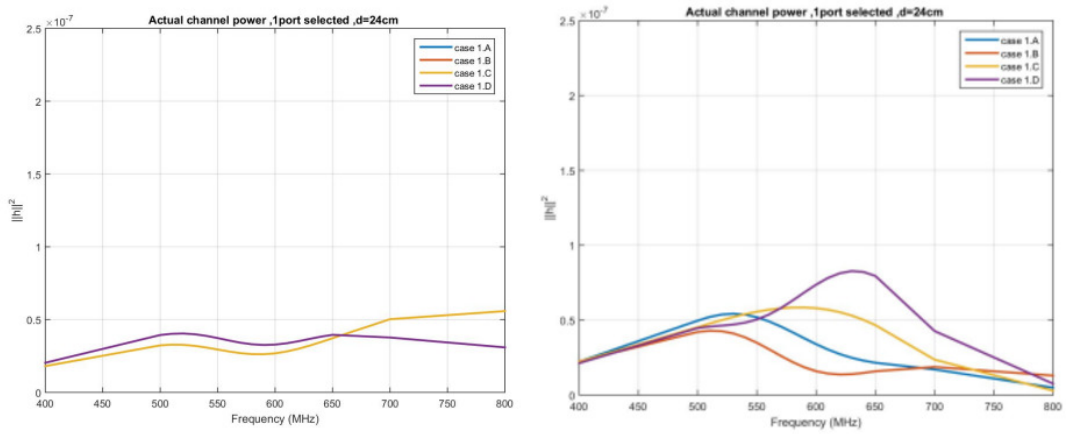

Figure 7.5: Actual Channel Power for 0°(left) and 45°(right)

Moreover, a critical observation is made. In contrast to the 0° study case, it is noted that in all of the 45° cases, the Conventional plot closely approaches or aligns with the Achievable plot without any notable differences. This significant finding indicates that a **45° angle is highly advantageous for transmission** because of the fact that, in all of the cases and distances (d), the antenna will achieve its **ideal performance**.

Metallic/Plasma Antennas 75°

Simulation Properties (2)

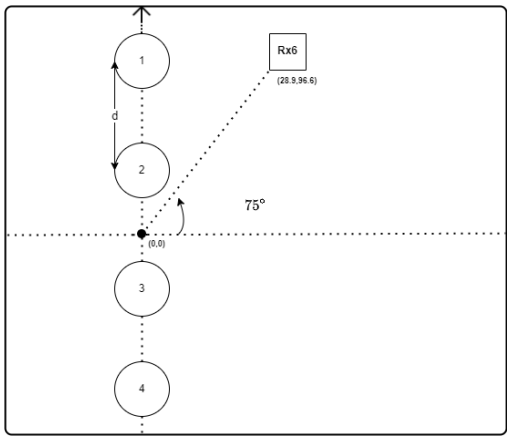

Simulations for $d = 12,\ 16,\ 20,\ 24$cm.

In the third experiment set, we perform our experiment on a receiver antenna located at x=28.9m, y=96.6m, and height z=3m and at 75°with the transmitter, which is located at x=0m, y=0m, and height z=3m, as can be seen in the figure above. The simulations will be for four distances d=12cm, 16cm, 20cm, and 24cm. Firstly, we will work on antenna selection for all the cases (all monopoles radiating, one monopole radiating, two monopoles radiating, and three monopoles radiating).

Our objective is to compare metallic and plasma antennas through various experiments and graphical simulations that we will analyze on the following pages for this particular case.

Channel power for different values of d.

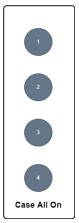

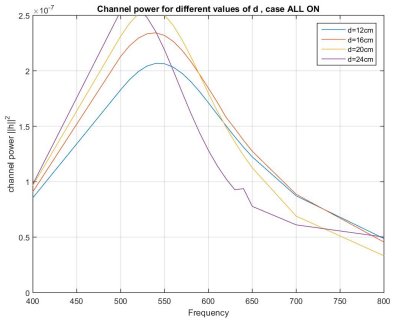

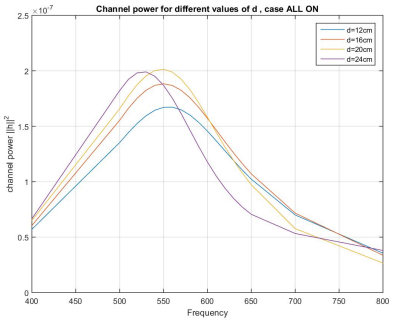

Channel power for different values of d. Case 1.A/1.B

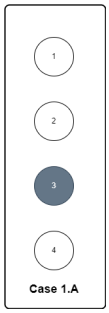

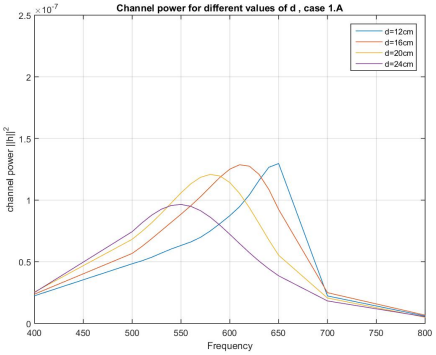

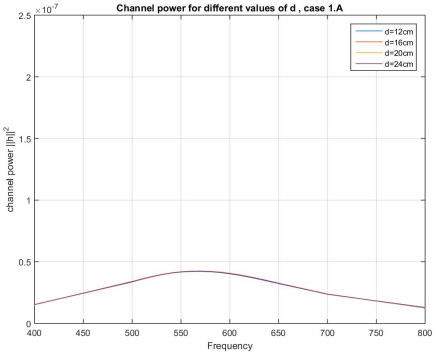

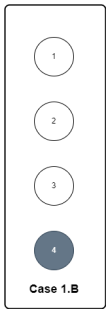

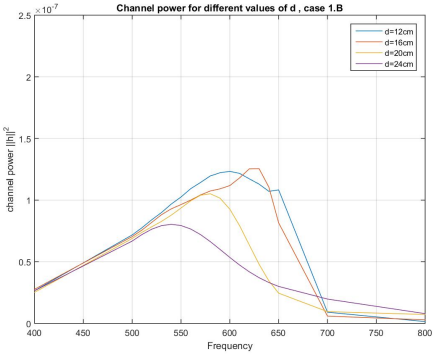

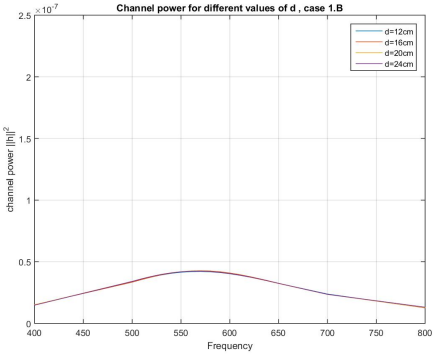

Channel power for different values of d.. Case 1.C/1.D

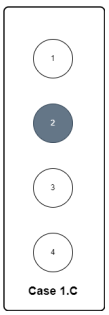

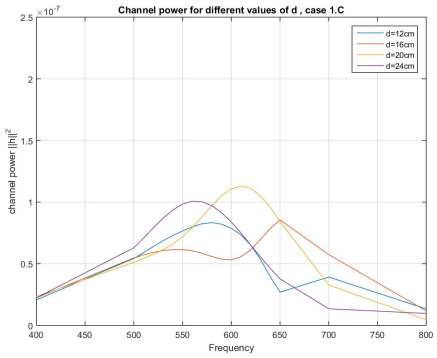

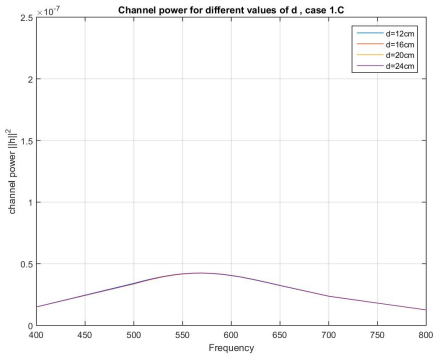

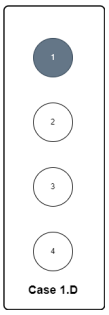

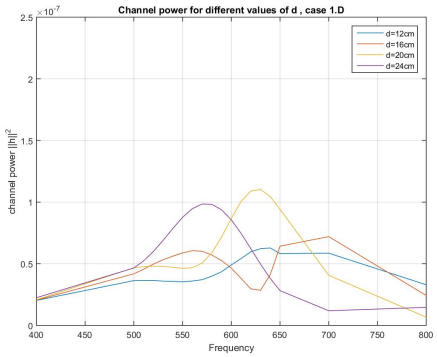

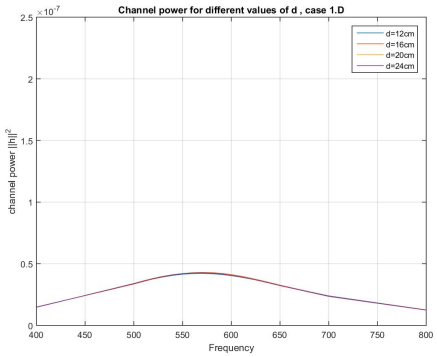

Channel power for different values of d. Case 2.A/2.B

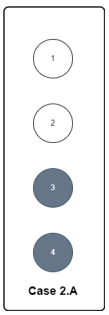

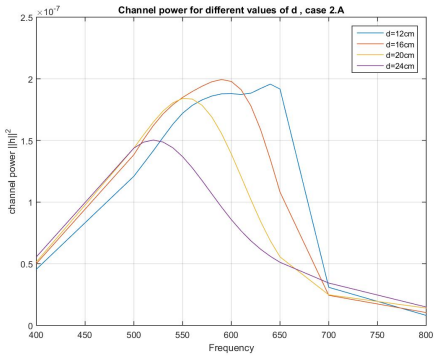

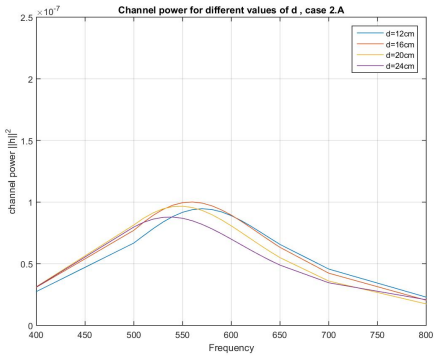

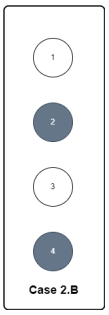

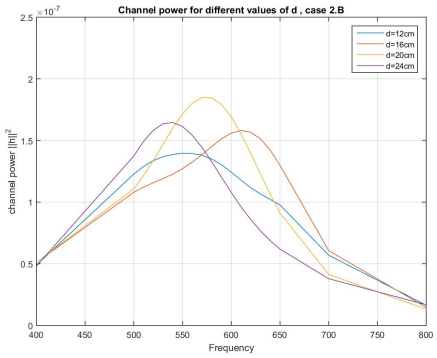

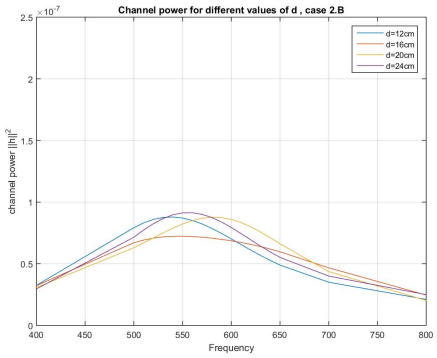

Channel power for different values of d. Case 2.C/2.D

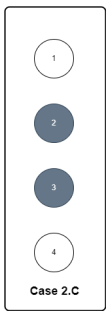

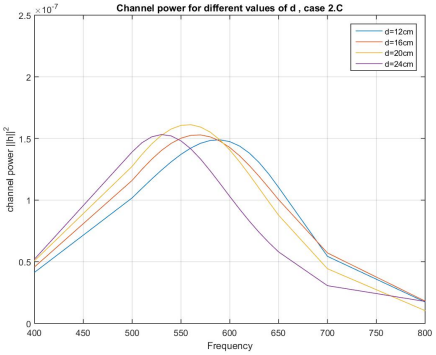

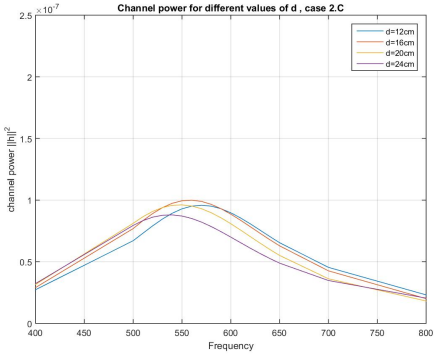

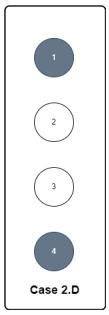

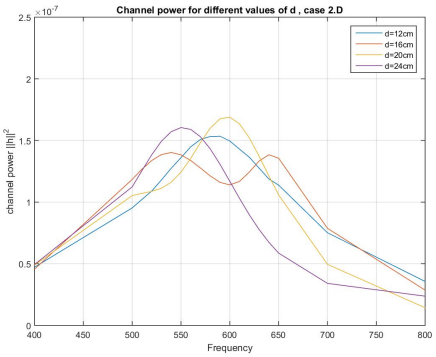

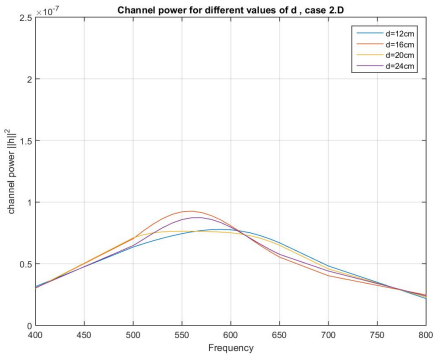

Channel power for different values of d. Case 2.E/2.F

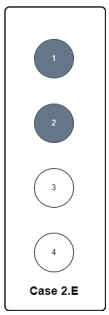

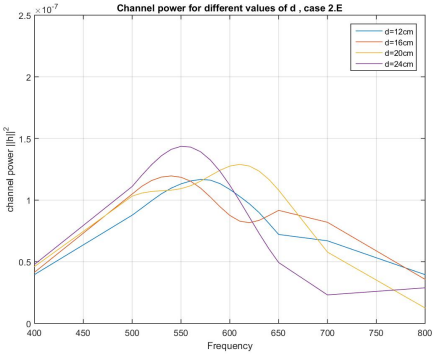

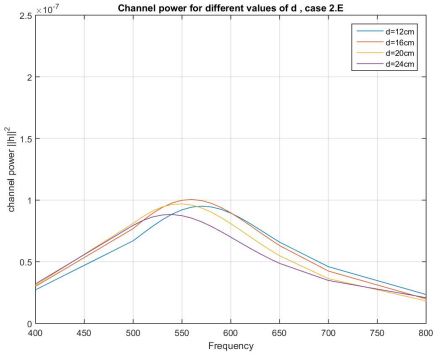

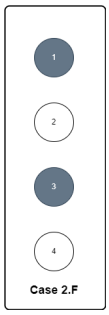

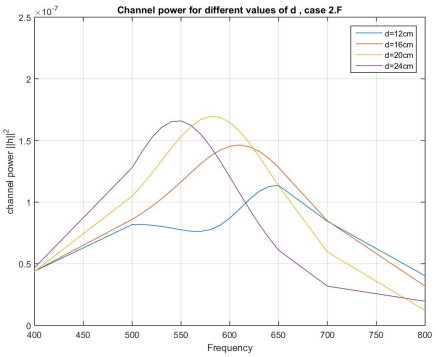

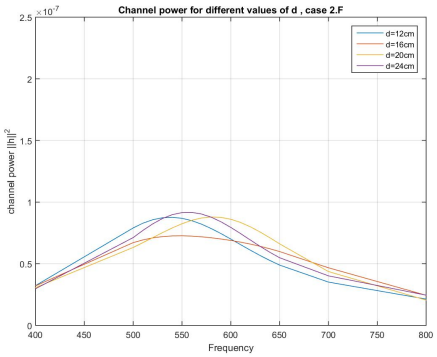

Channel power for different values of d.. Case 3.A/3.B

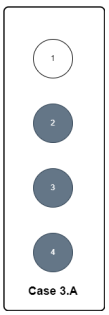

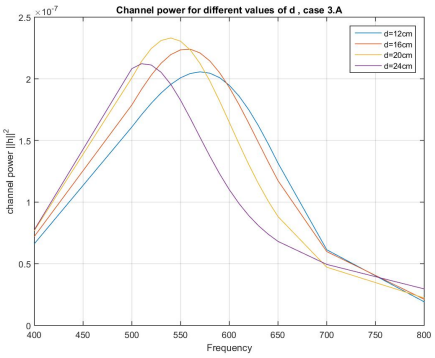

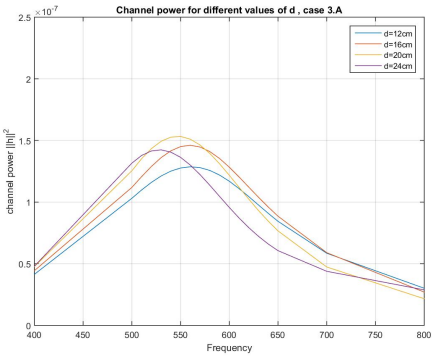

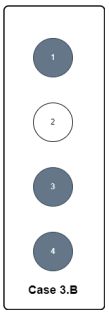

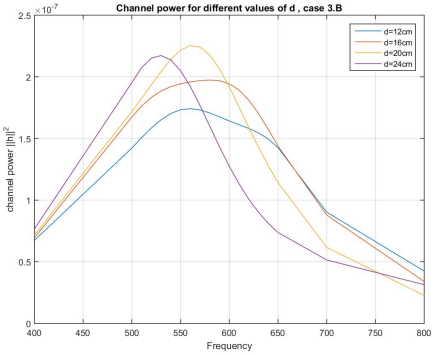

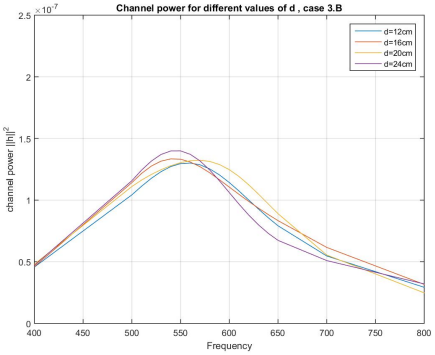

Channel power for different values of d. Case 3.C/3.D

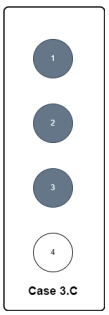

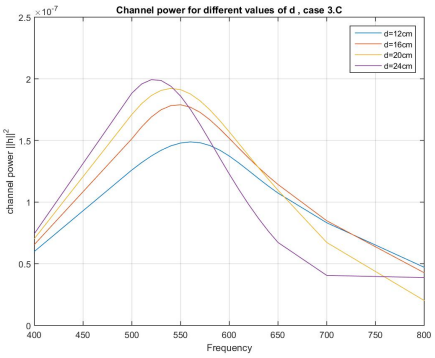

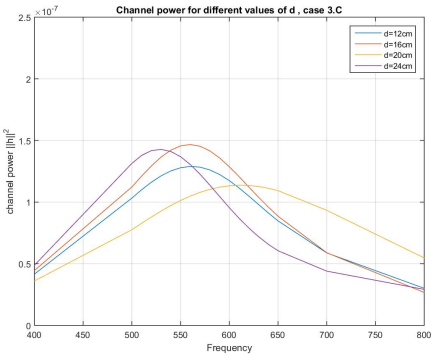

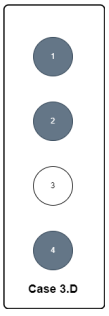

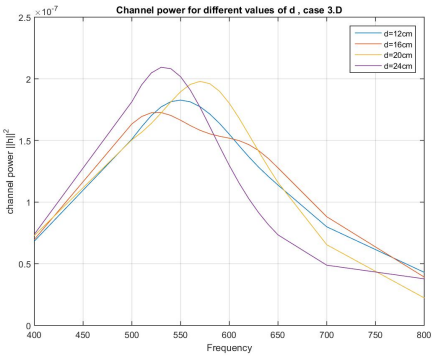

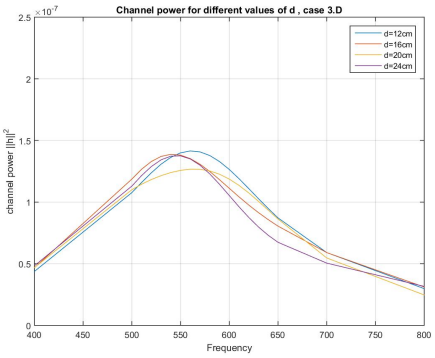

Many of the observations made in the context of the **30°** and **45°** cases also hold for the **90°** case. Our focus will be directed towards identifying the disparities and resemblances between these two scenarios, allowing us to discern the impact of receiver angle variations on transmitter antennas.

Our initial observation centers around the scenario where all ports are activated. In contrast to the 30° and 45° experiments, the graphical simulations exhibit notably higher channel power values, particularly for the metallic antennas. Upon comparing it with the corresponding plot at 0°, we can see that the peak channel power reaches almost double the value.

Shifting our focus, we delve into the other cases involving one port on, two ports on, and three ports on. Notably, significant irregularities and abrupt changes manifest in the plots for the metallic antennas. This indicates a pronounced dependency of channel power on frequency variations in the 75° study case for metallic antennas. Conversely, plasma antennas display more consistent patterns with minimal deviations from the other experiments.

Comparison of $\|\mathbf{H}\|^2$, 1 port selected, $d = 20\text{cm}$ (0.4λ).

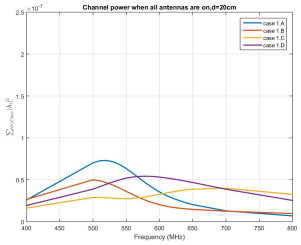

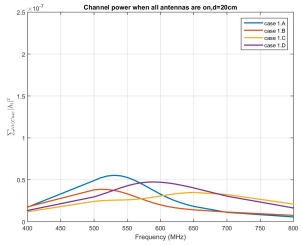

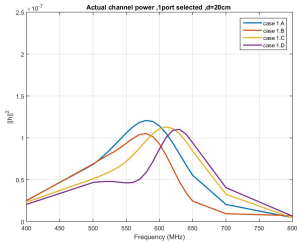

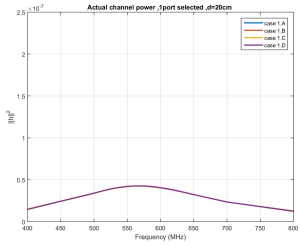

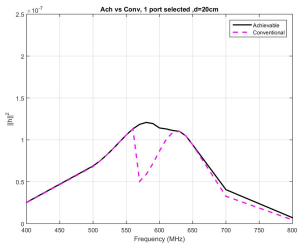

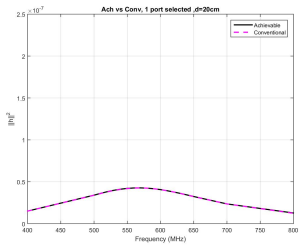

Comparison of $\|\mathbf{H}\|^2$, 2 ports selected, $d = 20\text{cm}$ (0.4λ).

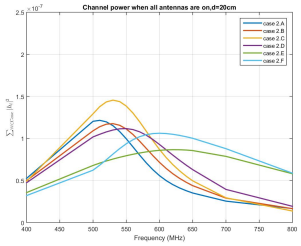

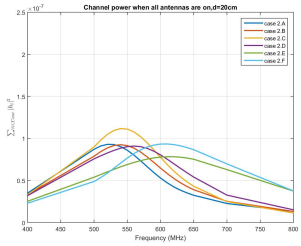

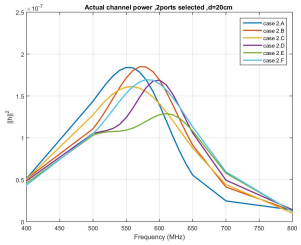

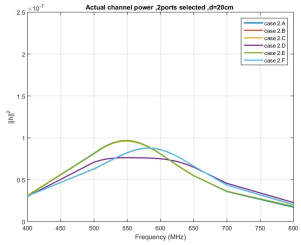

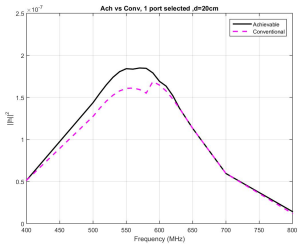

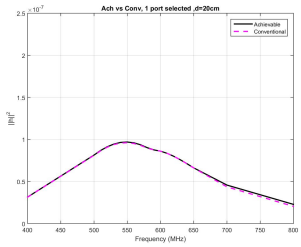

Comparison of $\|\mathbf{H}\|^2$, 3 ports selected, $d = 20\text{cm}$ (0.4λ).

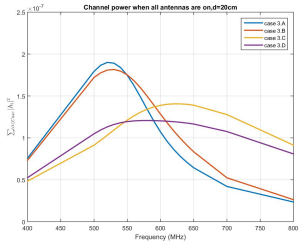

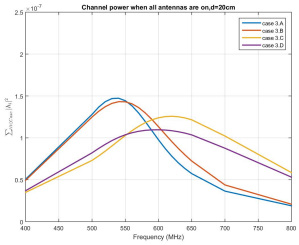

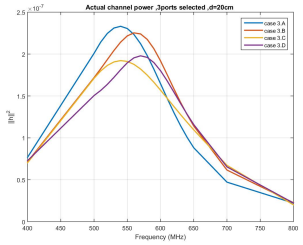

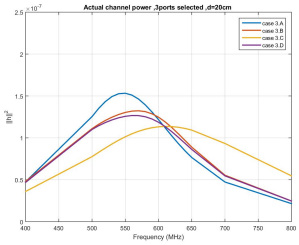

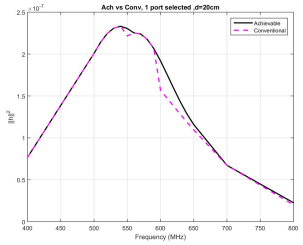

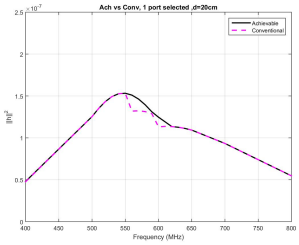

In the above experiments, we produce three different graphical simulations for both metallic and plasma cases:

- Channel power when all antennas are on
- Actual channel power
- Achievable vs. Conventional

The initial observation in this section revolves around the number of plots presented in the "Actual channel power" graph. In order to analyze this observation to a higher extend we will need the experiment result from the 0°case. In the 0° case (case where only one monopole is radiating), we observe the generation of two plots among the available four cases. Conversely, in the 75° case, there are four plots (same with the 45°case). This occurrence can be attributed to the symmetry of monopoles in the 0° case, producing identical plots. In contrast, the absence of symmetry in the 75° case leads to distinct plots. The same observation holds for the remaining two cases (two monopoles on, three monopoles on). Notably, in the case of two monopoles transmitting at a 75° angle, the "Actual channel power" graphical simulation produces six plots instead of the four observed in the 0° case.
In the Fig. 7.5 we can clearly see the above observation.

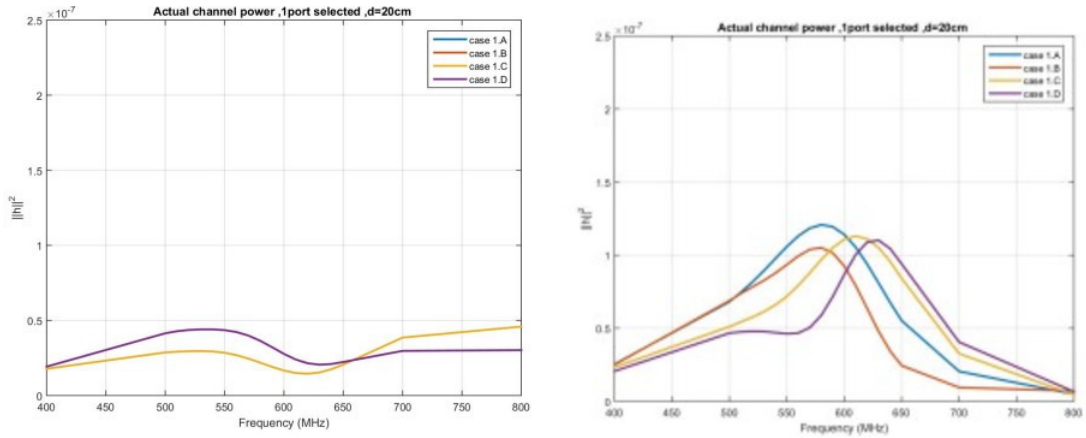

Figure 7.6: Actual Channel Power for 0°(left) and 75°(right)

Proceeding to our subsequent observations, it becomes apparent that for plasma antennas, the "Actual channel power" exhibits stability, with minimal abrupt changes observed in the plots. In contrast, metallic antennas generate volatile, unpredictable graphs characterized by oscillations and rapid fluctuations, as illustrated in Fig 7.7 below:

Figure 7.7: Actual Channel Power comparison for metallic(left) and plasma(right) cases

Moreover, we observe a substantial distinction in the channel power graphs in the case where three ports are activated. Specifically, the channel power plots for cases 3.A and 3.B exhibit significant differences compared to cases 3.C and 3.D, as illustrated in Fig. 7.8:

Figure 7.8: Channel Power comparison for cases 3.A, 3.B, 3.C and 3.D

In conclusion, we observe high values on the **"Actual Channel power"** plots especially for the metallic antennas. Consequently, this leads to higher values in the **"Achievable vs Conventional"** graphical simulations. Overall, we can deduce that when the receiver is positioned above the transmitter at a 75° angle, the actual channel power demonstrates increased magnitudes.

7.3 Metallic/Plasma Antennas channel power over degrees for frequencies 500MHz, 550Hz, 600Hz

This section aims to discuss the actual channel power of metallic and plasma antennas concerning specific frequencies, namely 500MHz, 550MHz, and 600MHz. As previously indicated in the introductory part of this chapter, the frequencies under consideration span from 400MHz to 800MHz with a fixed increment of 100MHz, except for the range between 500MHz and 650MHz, where a finer step of 10MHz is employed. The emphasis on this particular frequency range is critical for gaining a more comprehensive understanding of the frequency spectrum that warrants greater attention, given the finer resolution offered by the 10MHz step.

Thus, we will plot actual channel power over degrees for every study case (1 monopole on, 2monopoles on, three monopoles on) and d=20cm.

Channel power over degrees for $d = 20\text{cm}$ (0.4λ). Case 1.A/1.B

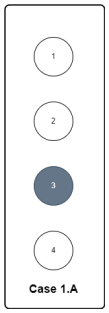

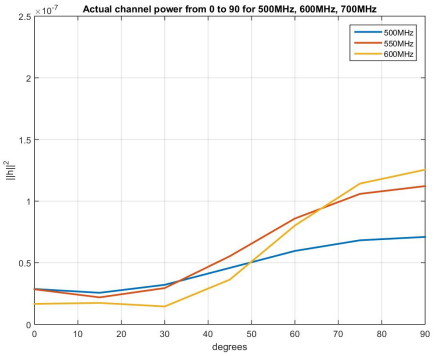

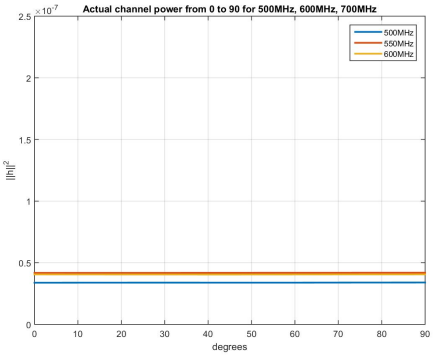

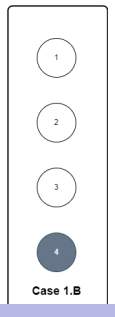

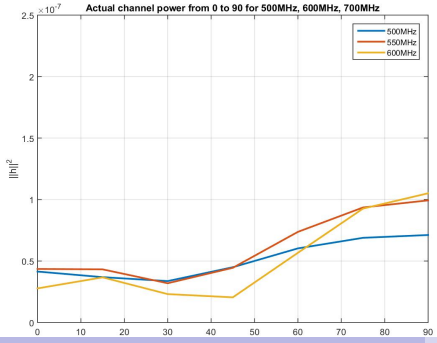

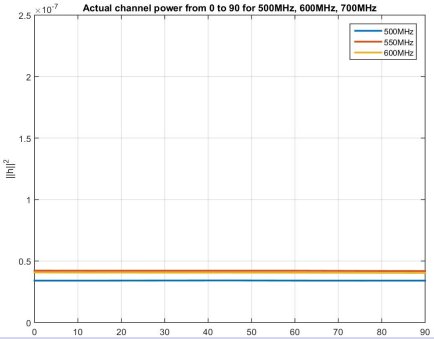

Channel power over degrees for $d = 20\text{cm}$ (0.4λ). Case 1.C/1.D

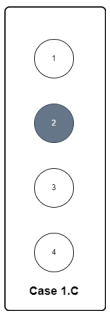

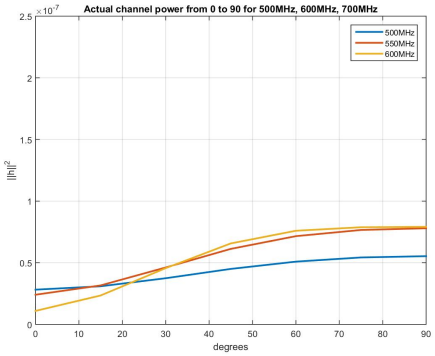

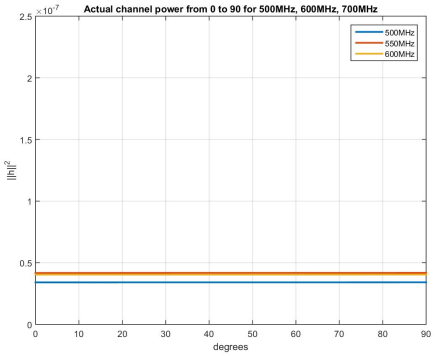

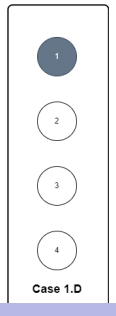

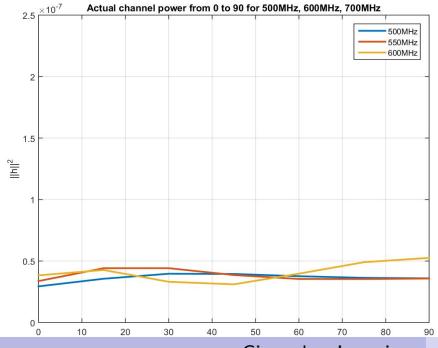

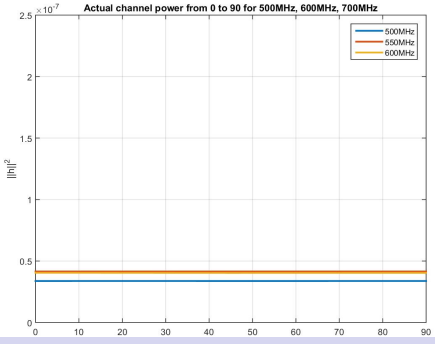

Channel power over degrees for $d = 20$cm (0.40λ). Case 2.A/2.B

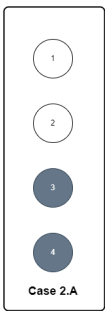

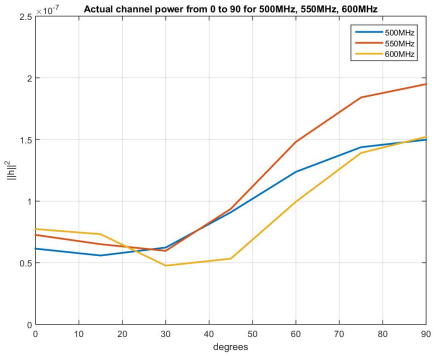

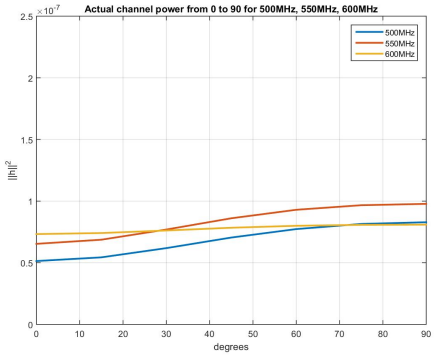

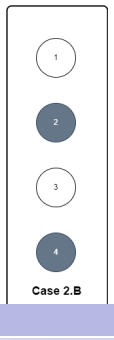

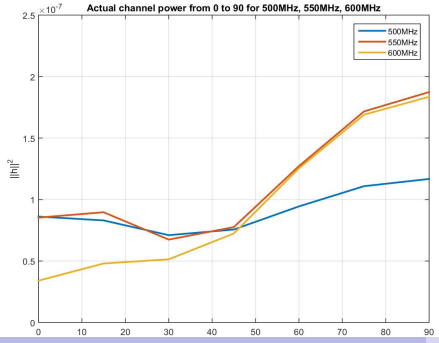

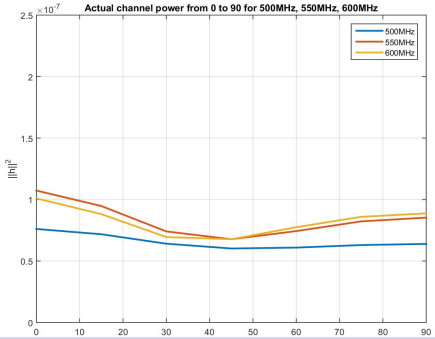

Channel power over degrees for $d = 20$cm (0.40λ). Case 2.C/2.D

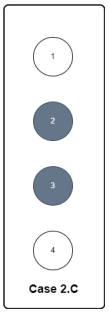

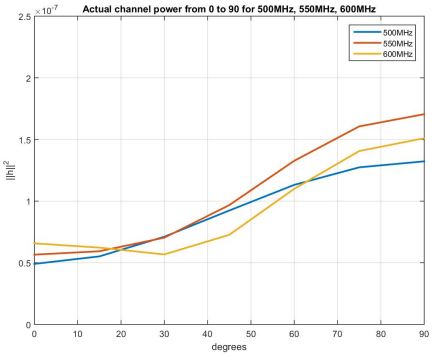

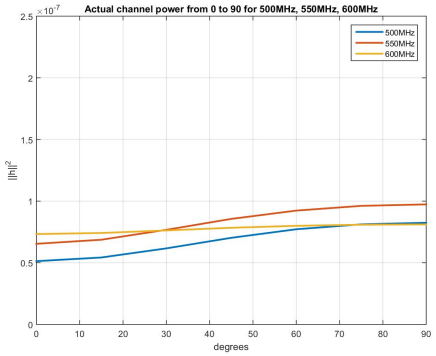

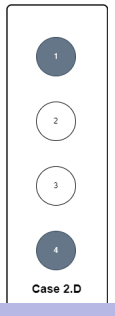

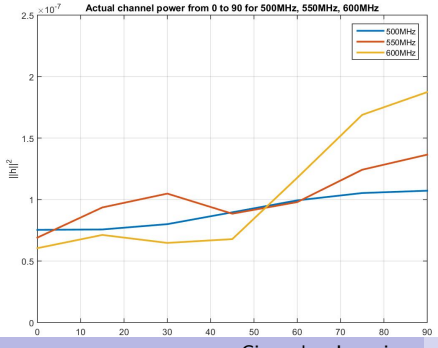

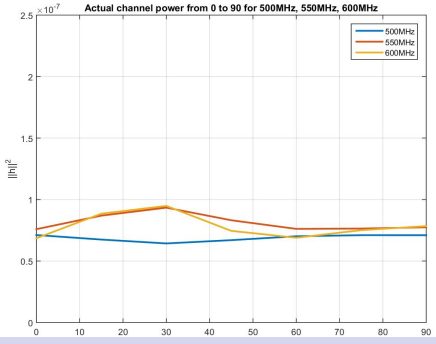

Channel power over degrees for $d = 20$cm (0.40λ). Case 2.E/2.F

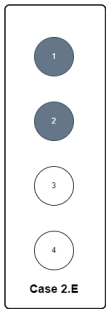

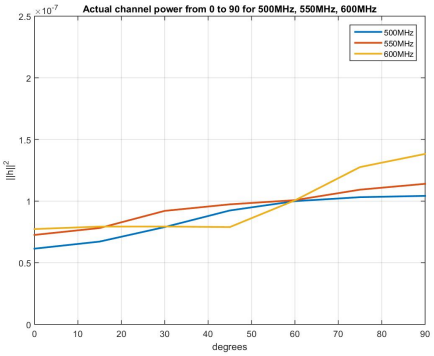

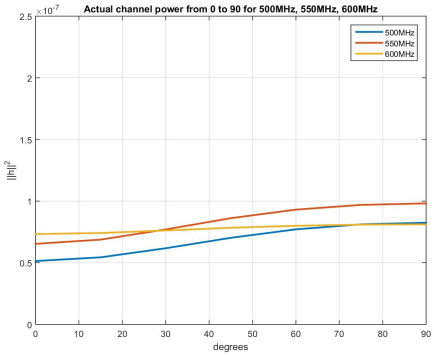

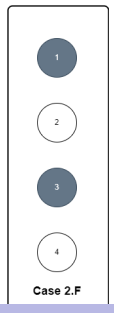

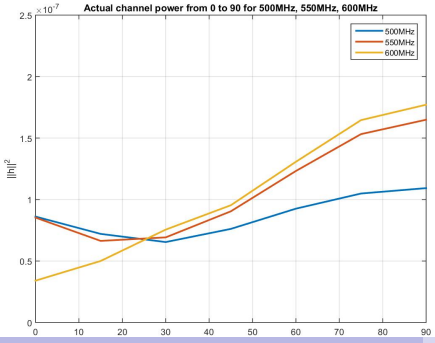

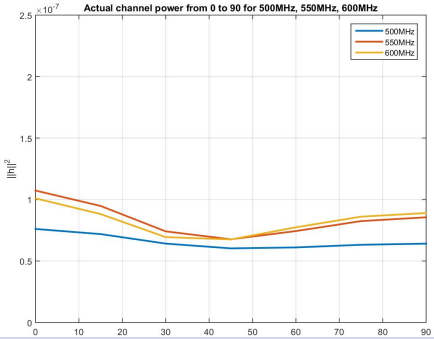

Channel power over degrees for $d = 20$cm (0.40λ). Case 3.A/3.B

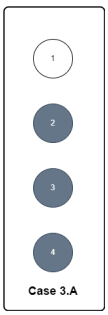

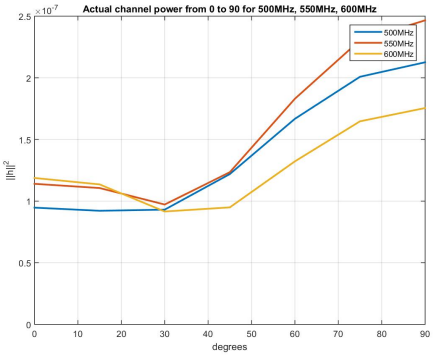

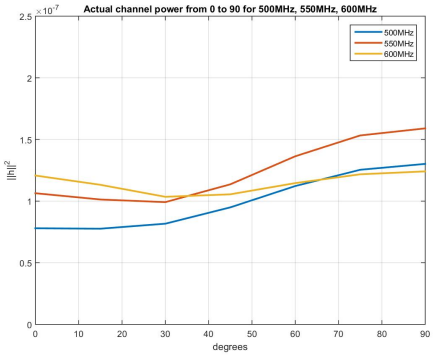

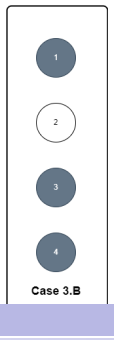

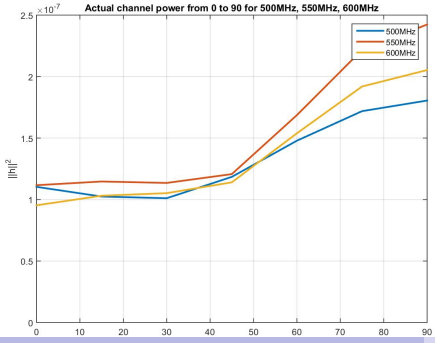

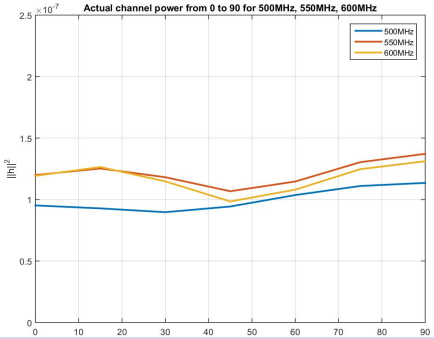

Channel power over degrees for $d = 20$cm (0.40λ). Case 3.C/3.D

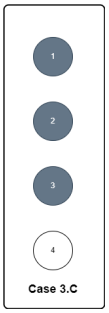

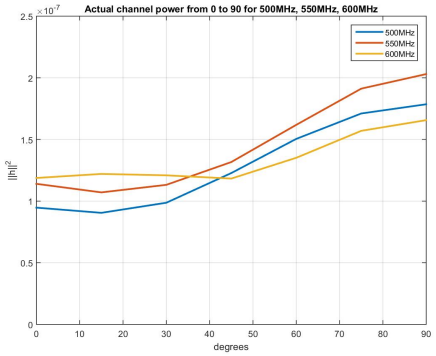

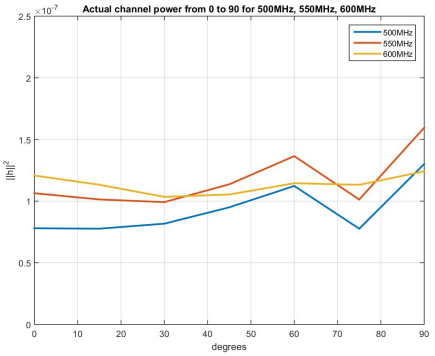

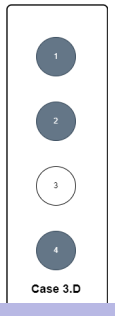

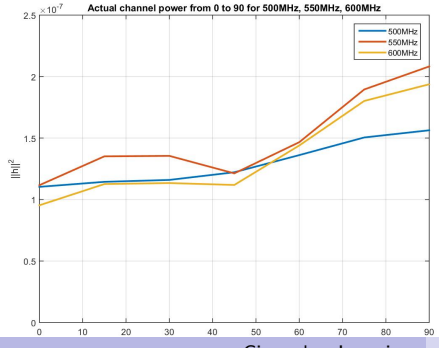

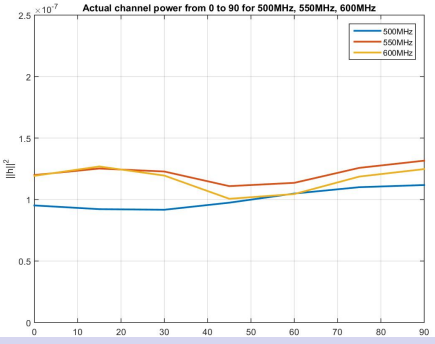

Remarkably, the above plots versus angle indicate that the metallic antenna performance depends strongly on the angle. At the same time, the plasma one is completely independent (although it performs mostly worse than the metallic one). Especially in the first study case, when one monopole radiates, plasma antennas produce straight lines for all three frequencies we study. Even if the radiating monopoles increase, the changes over the angle are insignificant. On the other hand, metallic behave differently. We can easily observe that when the angle increases, actual channel power increases for all study cases.

Moreover, for the below cases for the metallic antennas:

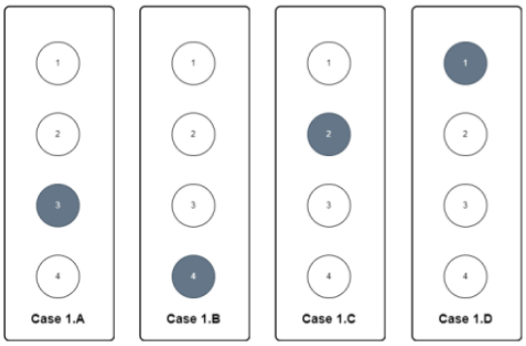

Figure 7.9: Study case one monopole radiating

We notice that case 1.A and 1.B have sharp and unstable plots, while cases 1.C and 1.D appear to have steady and gradually increasing changes, as illustrated in Fig. 7.10:

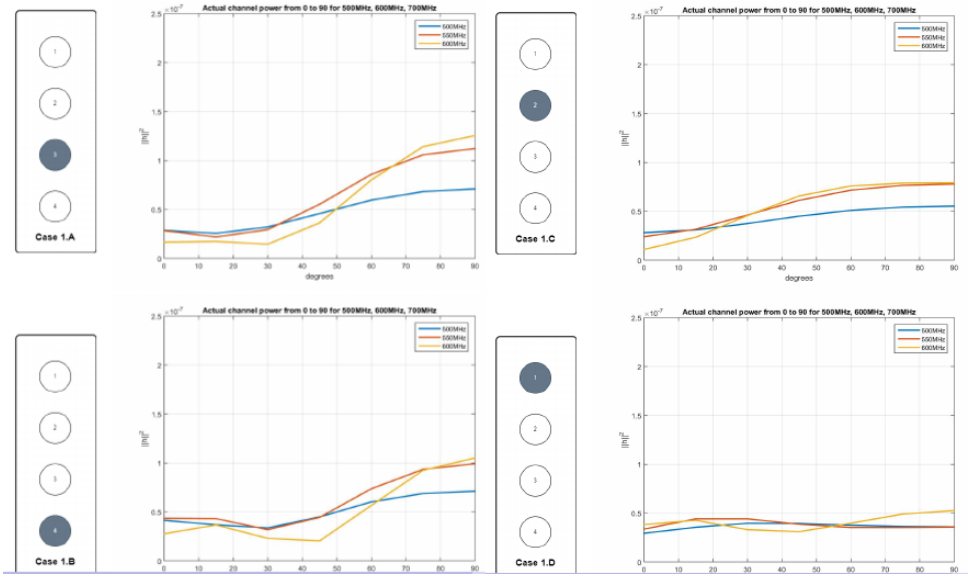

Figure 7.10: Difference between cases 1A,1B and 1C,1D

Furthermore, 500MHz plots have more stable schemes, and the change between the degrees is continuous. At the same time, 600MHz seems to depend significantly on the angle of all metallic cases where peaks and sudden changes are apparent.

7.4 Best performance based on channel power for 550MHz

In the last set of experiments, we will focus on the 550MHz plots from the last set. The main goal is to find which case performs better over the degrees for distance d=20cm. Thus, we plot all the cases of each study case together, and then we count which case has the highest channel power. To do that, we just mark the highest point in each degree case(0°, 15°, 30°, 45°, 60°, 75°, 90°), and we count which plot has the most points. The scheme with the most point performs best over the others. To provide specific details, we will create two plots for a focused frequency of 550MHz. On the left side, we will illustrate the actual channel power from 0° to 90°. On the right side, we will depict the graphical simulation showcasing the best performance. By doing so, we aim to present a comprehensive visual comparison between the actual measurements and the simulation results, enabling a clear assessment of the antenna's performance at the target frequency.

Moreover, this experimental procedure will be conducted for both plasma and metallic antennas. By performing this comparative analysis, we intend to gain a better and clearer understanding of our study cases concerning the focused frequency of 550MHz. The primary objective is to identify the best radiating case among the various scenarios considered, across the range of degrees. This comprehensive investigation will help us make informed conclusions regarding the optimal antenna configuration and its performance at the specific frequency of interest.

Case 1: Selection of 1 port.

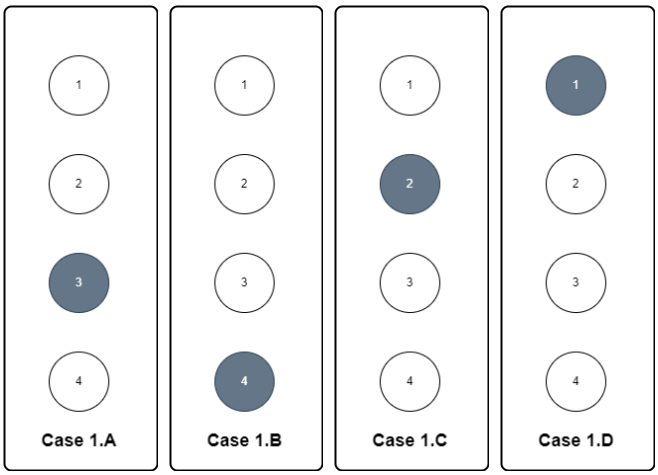

Best performance based on channel power for 550MHz and $d = 20cm$.

metallic

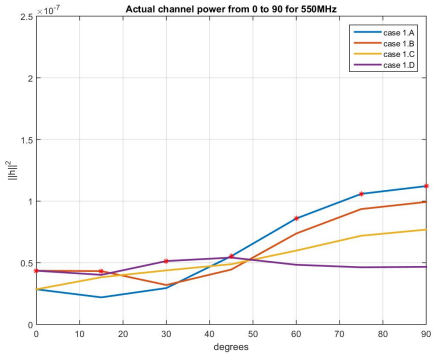

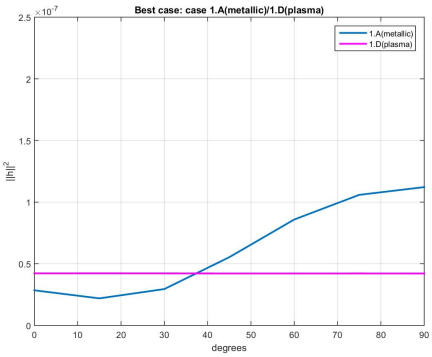

plasma

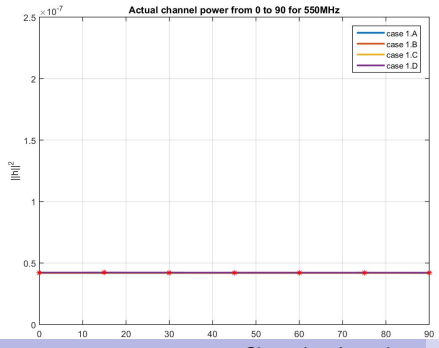

Case 2: Selection of 2 ports.

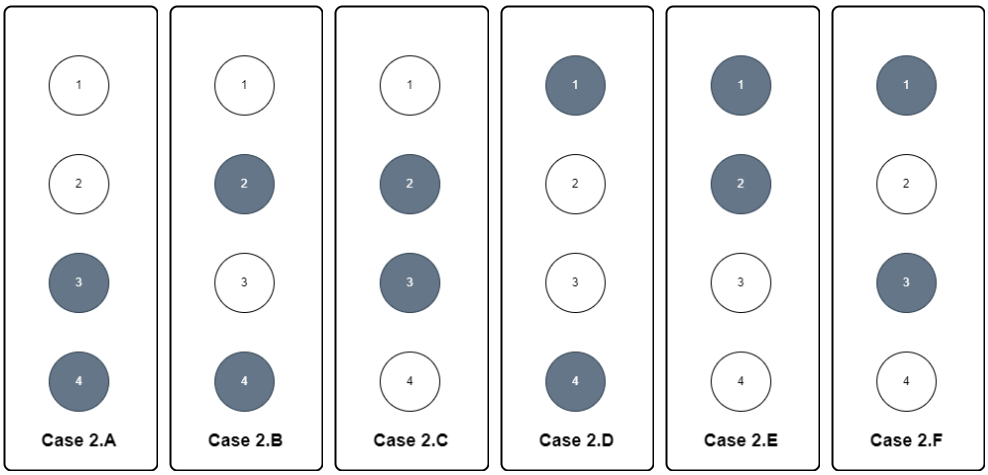

Best performance based on channel power for 550MHz and $d = 20cm$.

metallic

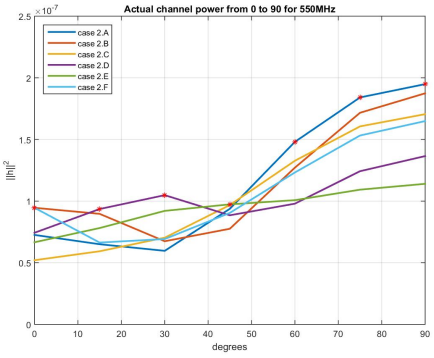

plasma

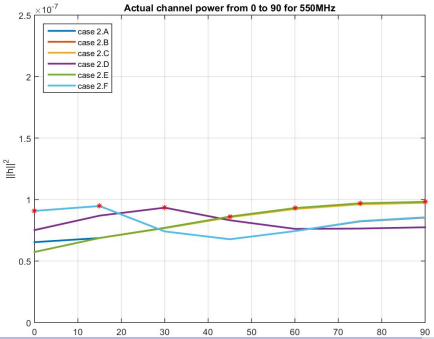

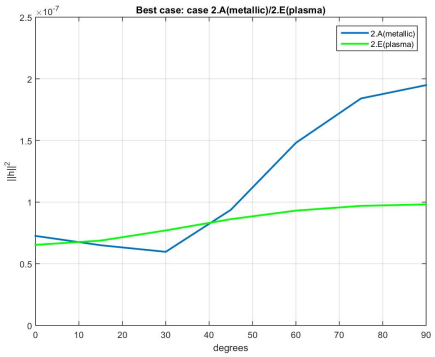

Case 3: Selection of 3 ports.

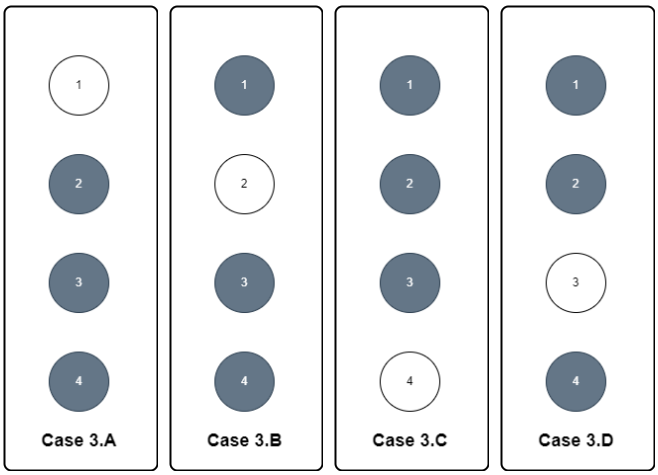

Best performance based on channel power for 550MHz and $d = 20cm$.

metallic

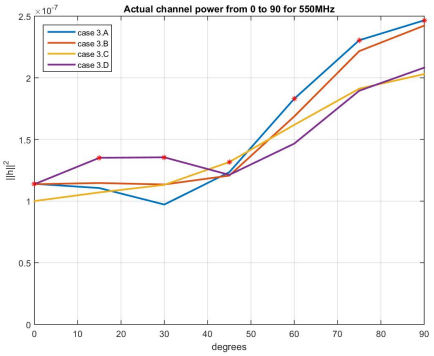

plasma

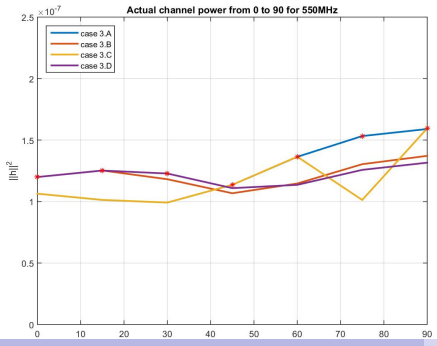

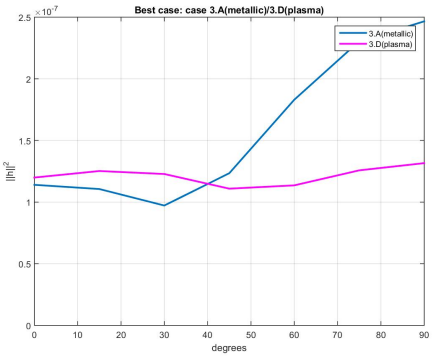

In most cases, especially on the plasma antenna ones, the differences between the cases are infinitesimals, and the mission to find which performs best often becomes challenging. In the first case(selection of 1 port) we observe that the four different plots are close to each other.

Especially concerning plasma antennas, we observed that the four different plots generated by varying cases are remarkably similar. In order to identify the superior performing case, we needed to closely scrutinize the values at each point, and this observation holds true for all the different distances we tested, not limited to the d=20cm case.

In contrast, as we moved to the other selection cases (e.g., activating 2 monopoles, 3 monopoles), the graphical simulations for plasma antennas started to exhibit more noticeable distinctions. For metallic antennas, the differences were significant, and we could readily discern which case performed better in most degrees just by examining the graphs. Furthermore, we noticed that although the plasma antennas' simulations remained relatively close to each other, the differences began to become more evident. In the final scenario, the disparities persisted, and we also observed an increase in gain.

In general, we noted that for degrees ranging from 0°-30°, plasma antennas tended to have larger channel power. However, for the remaining degrees, the channel power for metallic antennas experienced a substantial increase, while for plasma antennas, the channel power remained relatively stable without significant differences.

Bibliography

[1] WAI-KAI CHEN (2005) *The Electrical Engineering Handbook*

[2] S-parameters URL:https://www.antenna-theory.com

[3] Antenna Theory - Radiation Pattern URL:https://www.tutorialspoint.com

[4] Alkiviadis Vasilopoulos (2020) *MIMObit-assisted Antenna Selection*

[5] George Karystinos, Ioannis Grypiotis (2022) *Analysis and evaluation report of antenna simulation*

[6] George Karystinos, Athanasios Papadimopoulos (2022) *Antenna design and simulation*